

Measurement report: Rocket-borne measurements of large ions in the mesosphere and lower thermosphere – Detection of meteor smoke particles

Joan Stude^{1,5}, Heinfried Aufmhoff¹, Hans Schlager¹, Markus Rapp^{1,2}, Carsten Baumann¹, Frank Arnold⁴, and Boris Strelnikov³

¹German Aerospace Center (DLR), Institute of Atmospheric Physics, Oberpfaffenhofen, Germany

²Ludwig-Maximilians-Universität München (LMU), Atmospheric Physics, München, Germany

³Leibniz-Institute of Atmospheric Physics (IAP), Kühlungsborn, Germany

⁴Max-Planck-Institute for Nuclear Physics (MPIK), Heidelberg, Germany

⁵Royal Institute of Technology (KTH), Division of Space and Plasma Physics, Stockholm, Sweden

Correspondence: Joan Stude (joan.stude@gmail.com)

Abstract. We present mass spectroscopic, in situ data from rocket flights of two improved ion mass spectrometers in the mesosphere and lower thermosphere region. The instruments were optimized to detect large ions with mass-to-charge ratio (m/z , mass) of up to m/z 2000 and 20000 respectively, for analysis of meteor smoke particles. The flights were performed in the framework of the PMWE campaigns, initiated and coordinated by the Leibniz-Institute of Atmospheric Physics (IAP), to investigate polar mesospheric winter radar echoes in Andøya/Norway in 2018 and 2021. Both flights were successful and allowed to investigate the mass number and chemical composition of charged meteor smoke particles. We found a complex and diverse composition of positively and negatively charged molecules and particles within our mass range in a region that is notoriously difficult to get mass spectroscopic data from. While at altitudes below 85 km we observed negatively charged particles of up to several thousands of atomic mass units, above this altitude we found possible building blocks of these large particles that form right after their ablation from the parent meteorite material. In the first flight we detected no positively charged particles above m/z 100 and a difficult to interpret signal for negatively charged particles beyond our mass range of m/z 2000. In the second flight however, we detected positively charged particles between around m/z 180 and 350 and a number of different negatively charged particles up to m/z 5500. Due to the very large mass range of m/z 20000 used in the second flight and the subsequent lower mass resolution, unambiguous mass identification is not possible. A particular interesting pattern was found at 80.8 km of a compound that seems to double its mass around m/z 225, 450, 900 and 1800.

Comparing our findings to proposed meteor smoke particle compounds by other authors, our observations would be consistent with Magnetite, Fayalite and Forsterite. However, other possible compounds cannot be excluded.

1 Introduction

Meteor smoke particles (MSPs) range from molecule to nanometer sized particles that form due to ablation and re-condensing of meteoric matter upon entering the atmosphere (Rosinski and Snow, 1961). The high velocity of the impact causes the

parent material to heat up such that partial or complete ablation takes place at around 90 km altitude, in the mesosphere/lower-thermosphere (MLT) region. The gas phase particles react with background atmospheric ions to form larger particles with a peak layer around 85 km (Hunten et al., 1980). Although earlier measurements indicate a composition similar to chondrites (Zbinden et al., 1975), the actual composition of MSPs is subject to a number of studies (Antonsen et al., 2019; Hervig et al., 2017; Plane et al., 2014; Robertson et al., 2014; Obenberger et al., 2020) and is still an open subject (Plane et al., 2023) which require challenging measurements in the MLT region. As MSPs grow in size they act as electron sink and influence the charge balance of the region significantly (Baumann et al., 2015) before they sediment down (Megner et al., 2008). In summer the sedimentation process is enhanced as the temperatures in the mesopause region are low enough to allow larger water ice particles to form, with the MSPs as nuclei. During the winter month, the mesopause region is too warm for the formation of water ice and thus allows to investigate pristine MSPs in different stages of growth. The German Aerospace Center (DLR) has developed an improved ion mass spectrometer, jointly with the Max-Planck-Institute for Nuclear Physics (MPIK) and Ludwig-Maximilians-Universität München (LMU), which is based on an original design of MPIK with numerous deployments during rocket flights in the 1970s and 1980s (e.g., Schulte and Arnold (1992)). For the present purpose, two sounding rockets were equipped with this improved ion mass spectrometer, optimized for the detection of large ion clusters. The rockets were launched in the framework of two sounding rocket campaigns (PMWE1 / PMWE2) led by IAP Kühlungsborn in April 2018 and October 2021, with a total of 4 rockets. The campaigns aimed to study polar mesospheric winter echoes (PMWE) which are VHF radar echoes during the winter month at high latitudes (Latteck and Strelnikova, 2015). It was theorized that negatively charged MSPs may be involved in the creation of PMWE and indeed, as a result of the first flight, Staszak et al. (2021) could show that MSP enhance the radar echoes but that PMWE are ultimately caused by turbulence. Here we present the results from those two rocket flights for both, positive and negative ions, and discuss our measurements with regard to the detection of charged meteor smoke particles. Both flights took place in Andøya/Norway and an overview of the campaign and payloads is given in Strelnikov et al. (2021) and Staszak et al. (2021). In a previous paper (Stude et al., 2021) we introduced the instrument in detail, used during the first flight in 2018. In the present paper we will describe the technical improvements implemented for the rocket flight in 2021 (see Table 1). As in the previous paper we concentrated on selected mass spectra, we expand the discussion to the entire data sets of the rocket ascends of both flights in 2018 and 2021.

Table 1. ROMARA flights within campaign "PMWE"

Flight	PMWE1F	PMWE2F
Date	13 Apr 2018	1 Oct 2021
Launch time (UT)	09:44	10:03
Apogee [km]	121.4	126.7
Mass range [m/z]	≈ 2000	≈ 20000
Mass resolution (Xe)	17.4	5.8

Our instruments were able to obtain mass spectra between altitudes of 55 km to 121 and 127 km, respectively, during ascent and during descent, albeit then in the wake of the payload and thus with limited results. The instruments were calibrated to differently large mass ranges in order to analyze large ions ($m/z > 100$) and possible clusters of these, proposed by others (Schulte and Arnold, 1992; Gelinás et al., 1998; Lynch et al., 2005; Rapp et al., 2005, 2012; Strelnikov et al., 2012; Robertson et al., 2014; Havnes et al., 2015; Asmus et al., 2017; Chesworth and Hale, 1974).

In (Stude et al., 2021) we showed selected ion mass spectra from 55.7, 69.2 and 106.3 km altitude for positive and negative ions from the PMWE1F flight. Our major findings were that we have detected large negative ions with a mass-to-charge ratio (m/z , mass) of $m/z > 2000$ but no large positive ions. The largest masses we detected belonged to the expected proton hydrates (charged water clusters, Johannessen et al. (1972)) and the layer of iron ions.

We start this report with a description of the technical differences between the two instruments (ROMARA-1 and ROMARA-2) and their calibrations, followed by an overview of the data from both flights and a presentation of selected measurement details of interest. In the concluding section we discuss our measurements with regards to a possible detection of MSP compounds that have been proposed by: Rapp et al. (2012); Plane et al. (2014); Hervig et al. (2017).

2 The ROMARA instruments

The ROMARA (ROcket-borne MAss spectrometer for Research in the Atmosphere) instruments are cryogenically pumped, quadrupole mass spectrometers. These type of mass spectrometers filter ions according to their mass per charge (m/z), in between 4 electrode rods, assembling a high frequency, quadrupole electric field (Paul and Steinwedel, 1953). A subsequent channel electron multiplier then detects individual charged particles and produces small current pulses that are amplified and counted by the data processing unit. To produce a mass spectrum, the oscillator voltage at the quadrupole is gradually increased in mass channels and the respective counts are stored. A more thorough description is given in Stude et al. (2021) for ROMARA-1 and the PMWE1F flight. ROMARA-2 (flight PMWE2F) required changes that affected the aerodynamic performance and led to further small modifications. In Fig. 1 both instruments are shown side by side to illustrate these differences.

ROMARA-1 used a cryopump of 150 mm diameter to accommodate enough cryogen for the required time to wait on the launch pad for the desired atmospheric conditions. During refurbishment for ROMARA-2 we noticed a leak in the cryo system and attempts of repair did not meet the tight requirements of the vacuum system's leakage rate. We therefore used an alternative pump with 208 mm diameter from our shelves. This required adjustments in instrument geometry to avoid deterioration of the aerodynamic performance around the intake cone. Therefore, we improved the intake cone to a more pointier design with an opening angle of 60° instead of 82° as with ROMARA-1 to regain comparable aerodynamic performance and assure an undisturbed sampling of the atmosphere. Following the smaller opening angle of the intake cone, the quadrupole lens was lengthened by 13.3 mm to maintain same distance to the intake orifice. We further moved the channel electron multiplier up to increase detection efficiency.

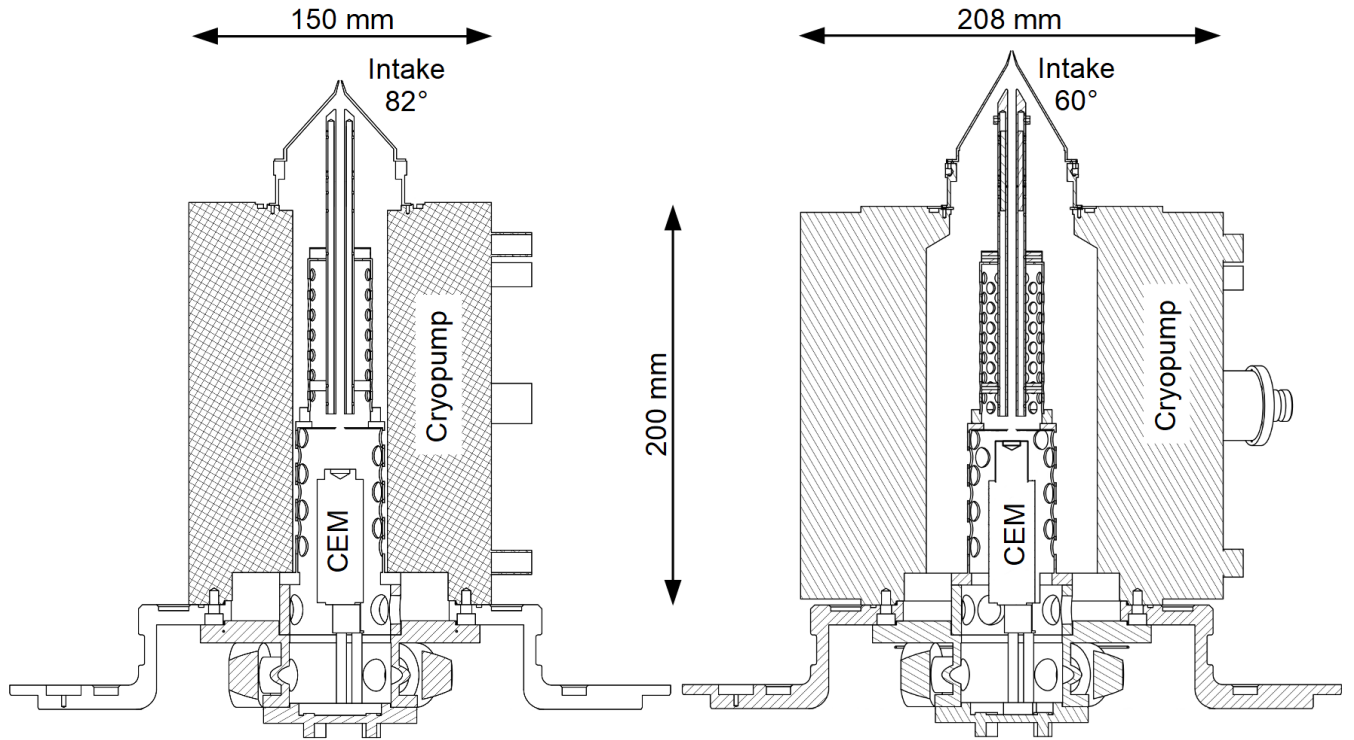


Figure 1. Technical drawings of the mass spectrometer ROMARA-1 (left) and ROMARA-2 (right) in their flight configuration.

2.1 Electronics

The electronics section of ROMARA-2 was modified as well with two major improvements: the control of the quadrupole oscillator and the amplifier to detect the channel electron multiplier pulses. For ROMARA-1 we used A111F from AMPTEK® as charge amplifier mainly for its sufficient performance and small form factor but realized that under certain conditions the count rate might exceed the limits of the A111F and thus we upgraded to the A121 from the same company. The A121 charge amplifier allows a higher count rate of up to 12 MHz and thus has a smaller minimum dead time of 80 ns (350 ns for A111F). For ROMARA the count rate is corrected for the amplifier dead time by:

$$85 \quad R_t = \frac{1}{R_m^{-1} - \tau} \quad (1)$$

with R_t as true count rate, R_m as measured count rate and τ as dead time. The second improvement concerned the control of the quadrupole oscillator as we wanted more flexibility for ROMARA-2. The high voltage RF oscillator amplitude V_{RF} is controlled by a single analog voltage V_c , such that $V_{RF} = GV_c$, with G being in the order of 250. As V_{RF} is linear proportional to mass, so is V_c :

$$90 \quad [m/z] = \frac{4eGV_c}{0.908r_0^2(2\pi f)^2} \quad (2)$$

with e as elementary charge, r_0 the radius of the imaginary circle between the rods of a quadrupole and f as the frequency of V_{RF} . As the mass resolution is roughly constant over the mass range, mass peaks or mass steps in the mass spectrum have an increasing width with higher mass settings. For a mass channel scanning with a constant step width, this means more and more mass channels are used on a peak or step at higher masses. This was the case for ROMARA-1, where a saw-tooth of 4096 voltage steps concluded in 4096 linear mass steps of roughly 0.5 u width. In the extreme case of m/z 2000 a hypothetical mass step at a mass resolution of $17.4 m/\Delta m$ is about 115 u wide, spending about 230 mass channels on it while for m/z 30 only 4 mass channels are used. This wastes precious measuring time on a sounding rocket flight. To achieve the same amount of mass channels per step over the full mass range a logarithmic control is required, especially for an instrument with even lower mass resolution such as ROMARA-2. For the given mass resolution of about 6 and a mass range of about m/z 20000 a total number of 64 logarithmic mass channels would cover the whole mass range. With the given dwell time of 300 μsec a single mass spectrum could thus be run in a fraction of the time, however the high voltage oscillator needs a certain time to settle the higher value and thus we decided for a conservative approach, leading to 256 mass channels for each spectrum with $8 \times 296 \mu\text{sec}$ dwell time, effectively cutting the acquisition time in half. Thereby we could keep the same data structure of the underlying data acquisition system and run two spectra in the given 4096 mass channels. Logarithmic mass steps thus allow minimizing the time needed for a complete mass spectrum without loss of information if the mass resolution allows it.

Table 2. ROMARA mass filter settings

	ROMARA-1	ROMARA-2
frequency [MHz]	1.4	0.5
max. RF voltage [V]	1750	1810
radius r_0 [mm]	2.13	2.13
mass channels	4096	256
dwell time [μsec]	300	8×296

2.2 Calibration of ROMARA-2

As we observed during the ROMARA-1 flight a substantial negative ion population with masses above m/z 2000 ($r \approx 0.7$ nm), we decided to increase the mass range for ROMARA-2 to about m/z 20000 ($r \approx 2$ nm; Stude et al. (2021)) by decreasing the oscillator frequency from 1.4 MHz to 0.5 MHz (see Table 2). This has the drawback of a reduced sensitivity and resolution, with initial tests in the lab showed about a factor 2 less sensitivity for krypton ions used for calibration. The mass resolution $m/\Delta m$ was reduced to about 6 for krypton and xenon ions, compared to 17.5 of ROMARA-1. Both instruments are operated in the RF-only mode for quadrupole mass spectrometers providing highest sensitivity. The RF-only mode produces spectra sometimes described as integral or high pass mode. In this mode, ideally all ions passing the mass filter at the beginning of a

spectrum and are gradually filtered out with the increasing oscillator voltage. The mass scan thus produces mass spectra with
115 negative steps where the count rate drops, until all ions are filtered out or the maximum voltage of the oscillator is reached.

In practice this behavior is not strictly an integral or cumulative spectrum but rather large mass windows that are moved
through the spectrum and for a reduced oscillator frequency this behavior is unfortunately amplified. At low mass settings
large ions do not respond well to the oscillator voltage and thus are not guided well through the quadrupole filter. As the
oscillator voltage increases, the ions are guided more efficiently as they respond better to the now sufficiently large fields and
120 form a peak before they get filtered out (see Fig.2 and Fig.3).

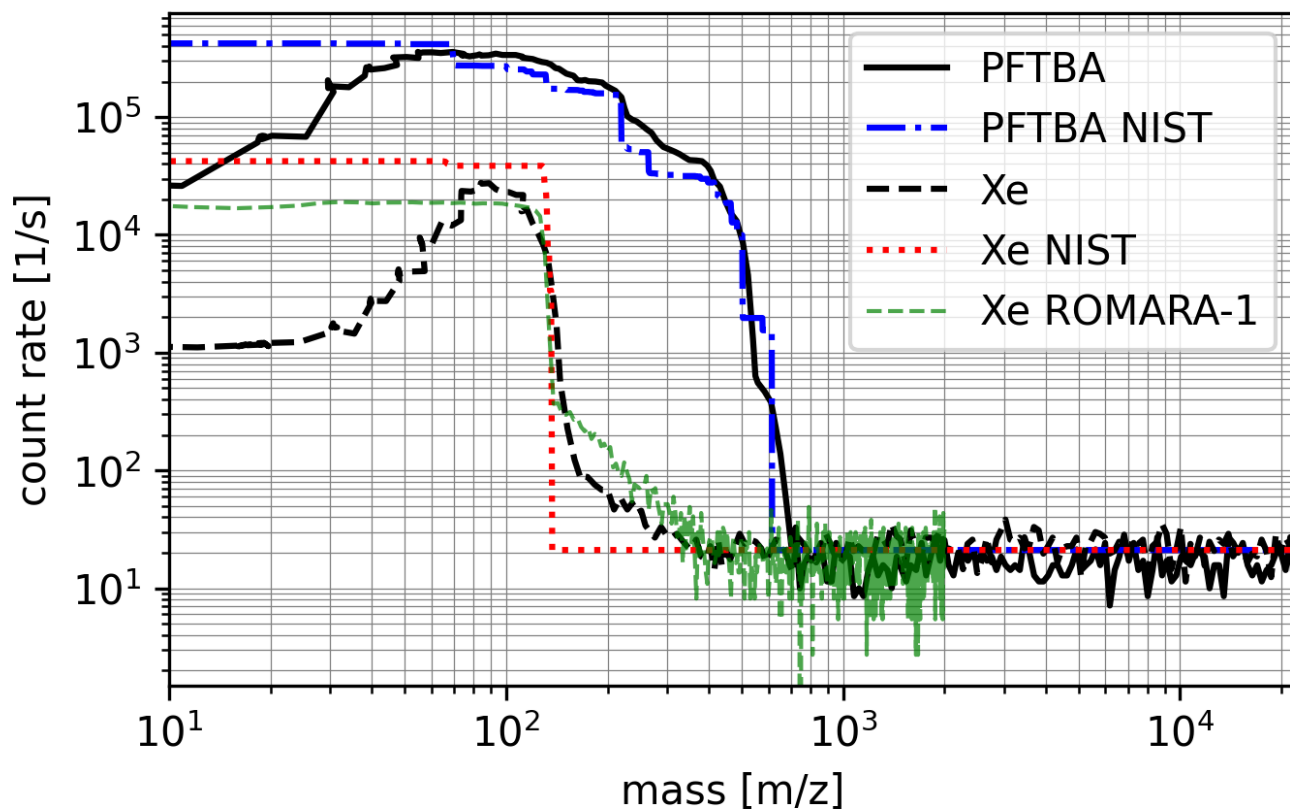


Figure 2. Mass spectra of ROMARA-2, for Xenon and PFTBA, the corresponding spectra from the National Institute of Standards and Technology (NIST) and a ROMARA-1 calibration for comparison

In Fig.2 we show the response of ROMARA-2 for xenon and PFTBA (Perfluorotributylamine or FC-43) ions, together with the NIST standard and a comparison to equivalent ROMARA-1 data. It is visible how some xenon ions pass at lower masses but form the aforementioned peak around m/z 80 before being filtered out at their respective mass per charge. The effect is similar on ROMARA-1, but to a much lesser extent. The xenon response for ROMARA-2 has a mass resolution $m/\Delta m$ at

125 50% FWHM of 5.8, while for PFTBA the mass resolution is between 4 and 8, depending on measuring mode and step size. In Table 3 the fits to the major steps of ROMARA-1 and ROMARA-2 calibration are given for comparison.

Table 3. Major steps of ROMARA calibrations

NIST [u]	ROMARA-1 [m/z]	ROMARA-2 [m/z]
131.3	130.9 \pm 3.8	123.7 \pm 17.4
219	218.2 \pm 3.4	220.2 \pm 18.4
264	257.6 \pm 13.8	259.1 \pm 54.9

For higher masses, we simulated the general behavior of how ions generate a peak in the RF-only mode of ROMARA-2 using SIMION[®] and one can see how these "mass windows" move through the mass range. Ions were simulated with an angle of attack of 5° and a cone distribution inside the intake orifice. The cone angle is determined as the vector from payload speed (1000 m/s) and thermal speed, i.e. large ions have a smaller cone angle. Each falling edge means ions are filtered out, while rising edges mean the mass filter becomes transparent for the respective ions and it is thus possible that edges might disappear as they cancel each other as shown in Fig. 3.

A further finding of the ROMARA-1 flight was a not well understood saturating effect of the count rate, possibly connected to very large ions, resulting in a dramatic dead time increase of the channel electron multiplier. To mitigate a possible saturation we decided to include a so called Mode B in the sequence of mass scans with a lower sensitivity by decreasing the bias potential of the quadrupole rods. ROMARA-1 had a bias of 20.5 and 50 Volt at the quadrupole lens and rods, which we call Mode A and was used in ROMARA-2 for keeping a comparable mode, that is used on both instruments. In Mode B the bias potentials were reduced to 5 and 12.5 Volt, see Table 4.

To prove the concept of Mode B and the general sensitivity of ROMARA-2 to large ions we tested the mass spectrometer in the laboratory with an electrospray ionization (ESI) source before integration of the instrument into the cryopump and the rocket payload. The ESI source was adapted to our laboratory setup from an "LCQ classic" ion trap (Thermo Finnigan). In this setup only the quadrupole/detector assembly and the electronics of ROMARA-2 could be used. Figure 4 shows mass spectra of a tuning liquid (Agilent Part Number: G1969-85000) of Mode A and B for negative ions. The ESI-L mass spectrum data from Agilent given in its respective datasheet (Fig.4) is limited to m/z 3200 and does thus not fully cover our mass range. For a confirmation of the ROMARA-2 mass spectra, i.e. the large tail above m/z 3000, a laboratory mass spectrometer with sufficient mass range would be required to interface in the same way to our setup which we did not have. The maximum major ion masses correlate quite well with the Mode B spectrum where the count rate declines at about m/z 3000 similar to the datasheet, although distinctive identification is not possible. Thus the results are only of qualitative nature but prove that ROMARA-2 is sensitive to ions of several thousand masses per charge and that Mode B provides some form of attenuation even if it is not constant over the whole mass range.

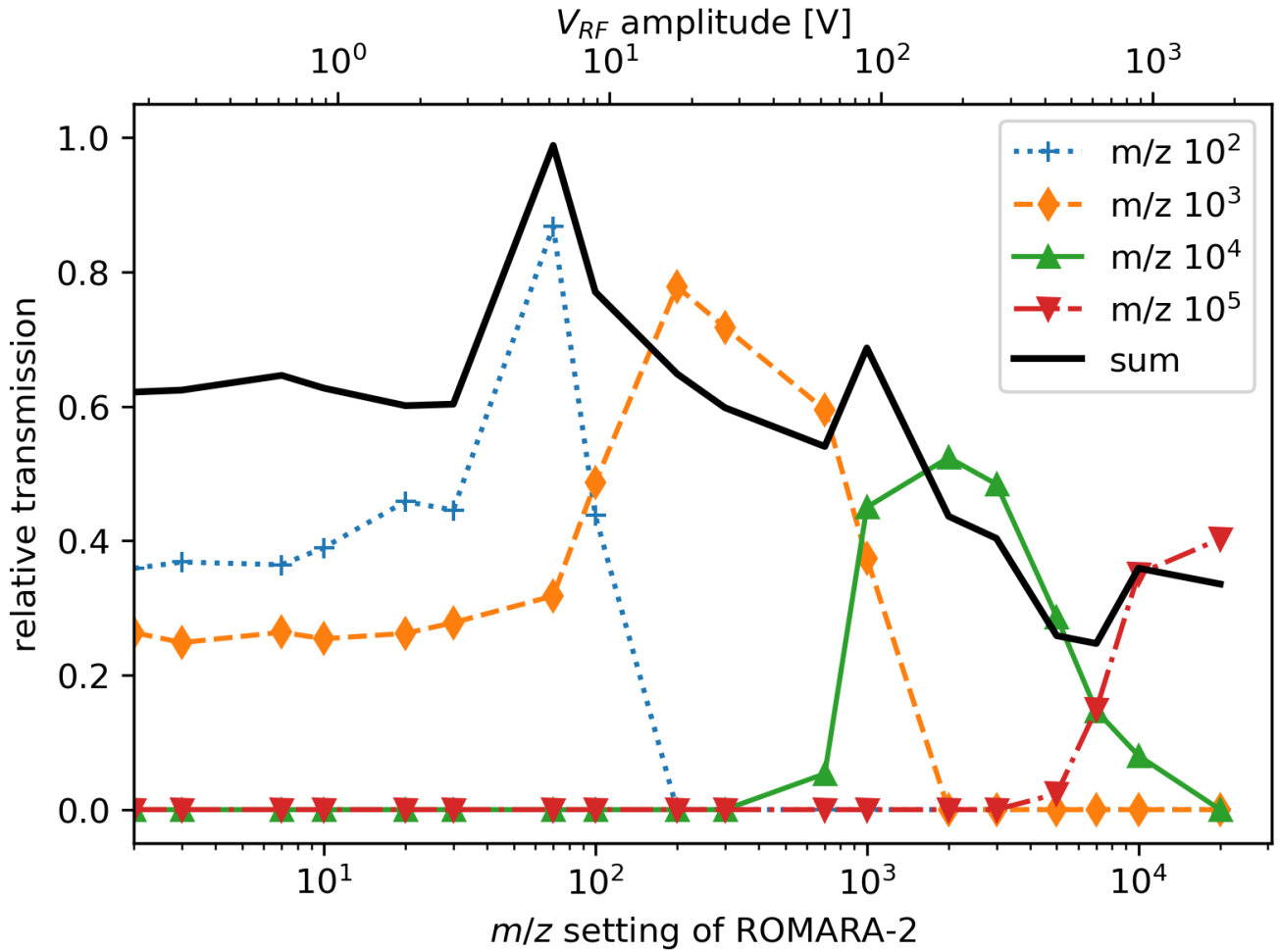


Figure 3. SIMION[®] simulation of ROMARA-2 mass response for large ions

2.2.1 Measuring modes and sequence

ROMARA-1 measured positive and negative ions in alternating order with the intake cone at payload potential and a spectrum time of 1.2 s. This seemed to have provided just enough altitude resolution for the major layers in the atmosphere during the corresponding flight. However the unbiased intake cone was a considerable risk as e.g. a negative payload potential prevents negative ions from entering the intake cone if their relative energy is below the payload potential.

For ROMARA-2 we implemented 8 different measuring modes: a positive and negative (p,n) mode, an intake cone potential of 0 (payload potential) or ± 5 V (0,5) and Mode A and B (A,B). Thus the notation, e.g. "p5B" means positive ions, at -5 V intake cone potential in Mode B (Table 4). This notation will be used throughout the paper. As the payload charges up during flight a bias voltage on the intake cone helps ions to overcome the payload potential. Although 8 measuring modes

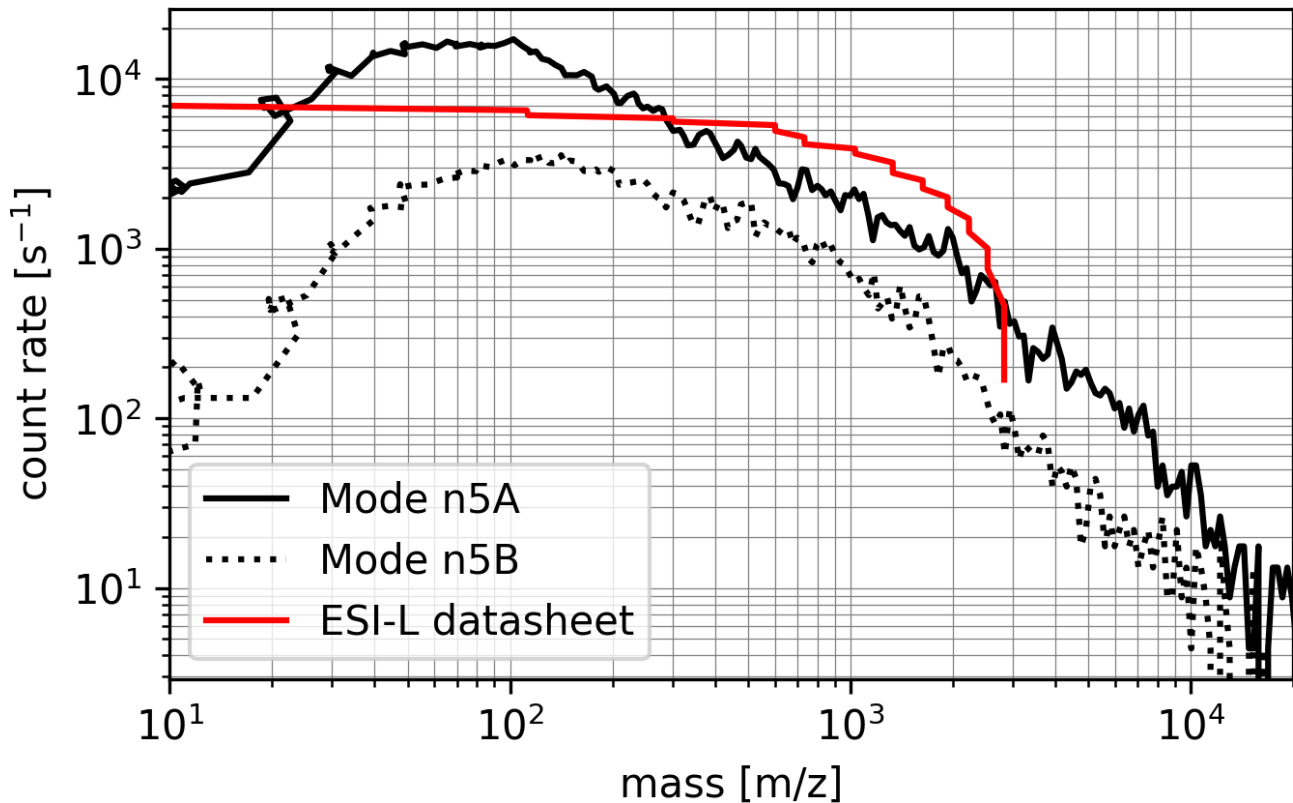


Figure 4. Negative ion mass spectra of the ROMARA-2 quadrupole with an electrospray ionization source (Thermo Finnigan), using ESI-L Low Concentration Tuning Mix from Agilent.

Table 4. Bias potentials for ROMARA-2

mode	p5A	p0B	n5A	n0B
intake cone [V]	-5	0	+5	0
quadrupol lens [V]	-20.5	-5	+20.5	+5
quadrupol rods [V]	-50	-12.5	+50	+12.5

160 seem to severely decrease the altitude resolution we considered it necessary, as it might help to improve the understanding of ROMARA-1 data. As an illustration, we show the measuring sequence at around 87 km altitude of ROMARA-2 in Fig. 5. The different modes are lined up as follows: n0A, n5A, p0B, p5B, n0B, n5B, p0A, p5A. The example also shows the effect of the payload potential as the payload apparently charges up negatively and thus prevents negative ions of being detected

during "n0A" and "n0B" mode. With a spectrum time of around $600 \mu\text{sec}$ and a payload speed of 1000 m/s (73 km) an altitude
 165 resolution of around 600 m is achieved repeating every 4.8 km .

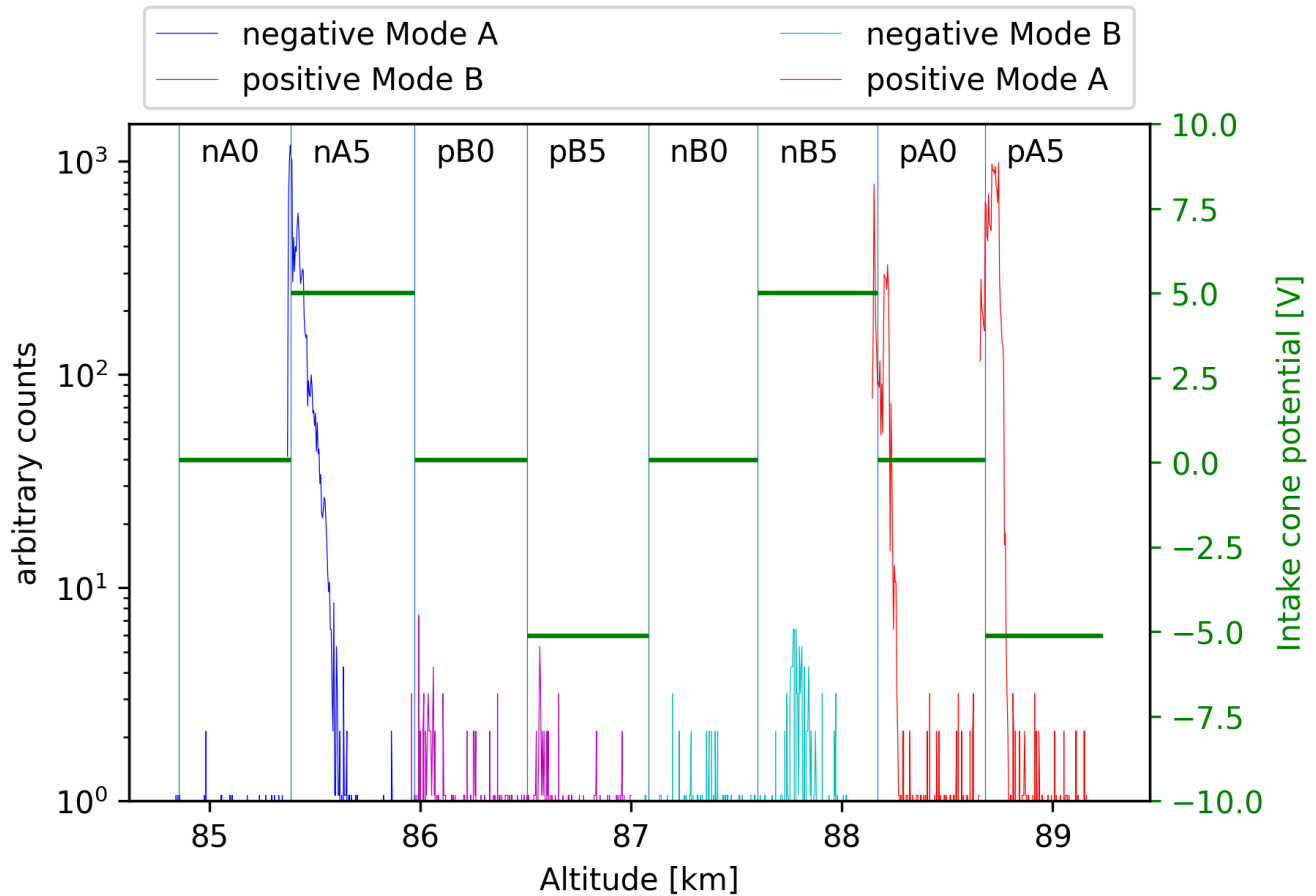


Figure 5. Sequence of measuring modes for ROMARA-2 around 87 km altitude. Negative payload charging prevents ions to enter the instrument in the "nA0" mode. See also Table 4.

3 Measurements

3.1 Rocket launches

ROMARA-1 was launched on 13th April 09:44:00 UTC into the tail of a polar mesospheric winter echo tracked on sight by the local radar (MAARSY) between 78 and 80 km altitude. While passing the natural echo, the payload of PMWE1F created an
 170 additional artificial echo as reported in Latteck et al. (2019). The same artificial echo was reported for PMWE1D for the 18th of April 2018. The launch of ROMARA-2 on PMWE2F took place on 1st of October 2021 at 10:03:00 UTC into a relatively

large and prolonged echo between 65 and 70 km, this time no artificial echoes were detected. The second payload PMWE2D was launched 3 minutes later. The launches and measurements of all instruments on both payloads were flawless and produced expected data. However due to a parachute failure on PMWE2D, only the PMWE2F payload could be recovered from the
175 Norwegian sea.

3.2 Positive ions ROMARA-1

The measurements of ROMARA-1 have been partly described in Stude et al. (2021) for 3 selected cases at 55.7, 69.2 and 106.3 km and are here covered as whole data set for the ascent (Fig. 6). The positive ion measurements show a somewhat expected result of light ions ($m/z < 100$) with 3 key features: proton hydrates (charged water clusters) up to 82 km with orders
180 of 3 and 4 water ligands [55u/73u], an ionized iron layer [56u] and NO^+ [30u] or O_2^+ [32u] above that. Minor steps in the spectra between 40 and 50 can be attributed to $\text{NO}^+(\text{H}_2\text{O})$ [48u] for the altitudes of proton hydrates and $\text{MgO}(\text{H})^+$ [40/41u] at around 90 km. Some counts at our threshold limit indicate ions up to around $m/z > 100$ but in general no heavier positive ions could be detected. Figure 6 shows these color coded, RF-only mass spectra between 55 and 115 km altitude during ascent of
185 ROMARA-1. The upper panel shows the full mass range up to $m/z > 2000$ with omitted negative measurements, while the lower panel is restricted to $m/z < 110$ and the omitted negative measurement slots are filled with positive measurement data to improve visibility.

3.3 Positive ions ROMARA-2

The positive ion measurements of ROMARA-2 did show expected light ions of below $m/z < 100$ and in contrary to ROMARA-1, some unexpected signals above $m/z > 100$, notably around 97 km, with masses up to about $m/z > 400$. In the upper panel of Fig.7
190 we plot all positive measurements at their respective altitude at the full mass range with the negative measurements blanked out. In the lower panel we restrict the mass range to $m/z < 400$ and filled the omitted negative measurement slots with the closest positive data to provide a better visibility, similar to Fig.6. Further measurements of Mode A at 0 V cone bias are marked in the plot as horizontal lines to indicate the sequence of the four different measurement modes (pA0, pA5, pB0, pB5) for each charge state.

195 The expected strong NO^+/O_2^+ peak was less dominant compared to ROMARA-1 but is still visible despite the much larger mass range and the resulting difficulties in calibration at very low masses. A similar pattern as with ROMARA-1 exists in the general mass distribution. Below about 88 km the ions are heavier as proton hydrates are present. The spectrum then becomes slightly lighter for the dominating Fe^+ [56u] and above about 100 km the step of NO^+ [30u] or O_2^+ [32u] dominates. However for ROMARA-2 the proton hydrates seem to be much heavier up to about $m/z > 150$ at 80 km, indicating orders of 8 or 9 water
200 ligands as reported by Björn and Arnold (1981). The striking feature, albeit with low count rates, are the large positive ions around 97 km just above the iron peak with masses between $m/z > 180$ and 350. As proton hydrates at those altitudes do not form (Reid, 1977) we assume that we have detected positively charged MSPs.

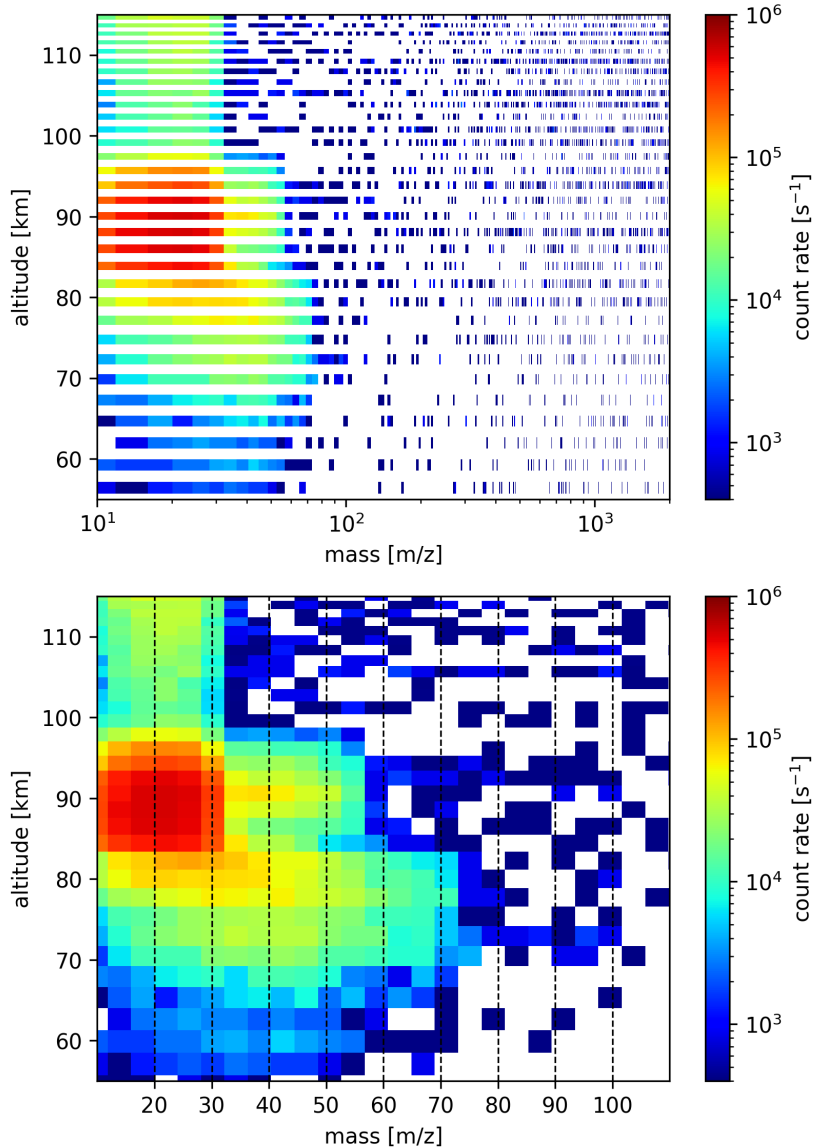


Figure 6. Positive ion spectra (8ch. mean) during ascent of PMWE1F (ROMARA-1). Upper panel with full mass range and logarithmic mass scale, lower panel with linear mass scale, reduced mass range and the negative measurement slots are filled with positive ion data for better visibility.

3.4 Negative ions ROMARA-1

The measurements of negative ions from ROMARA-1 (Fig.8) show a completely different picture compared to the positive
 205 ions, as our instrument was either too sensitive in the negative channel or the atmosphere contained a large number of negative

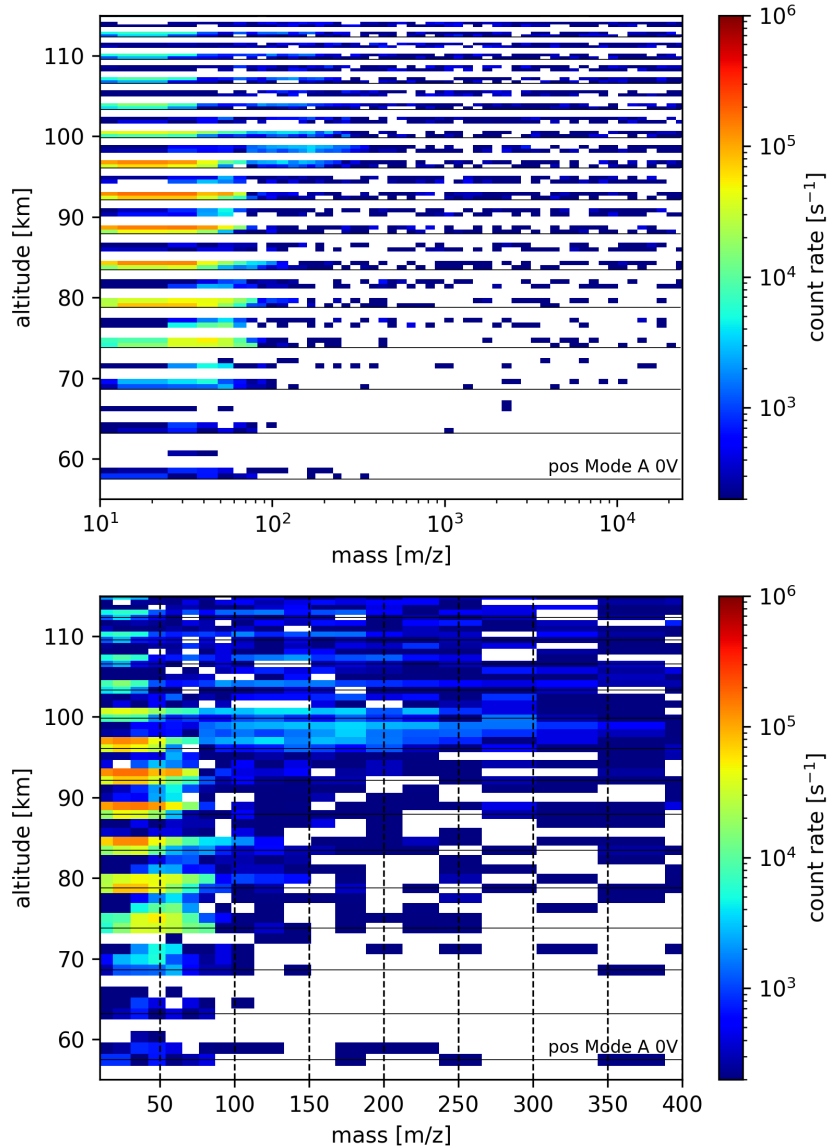


Figure 7. Positive ion spectra (32ch. mean) during ascent of PMWE2F (ROMARA-2). Upper panel with full mass range and logarithmic mass scale, lower panel with linear mass scale, reduced mass range and filled negative slots for better visibility. The horizontal lines mark the pA0 measurement to indicate the measurement sequence (pA0, pA5, pB0, pB5).

ions heavier than m/z 2000, that obscured our measurements. First, the moment of the cap ejection is clearly visible as large negative ions immediately enter into the instrument, as shown in the first spectrum at the bottom of Fig.8. For the next 20 km of ascent the signal of large ions is generally rising, modulated by the payload spin and then starts to saturate from about 75 km, up to about 100 km. The payload spin period is 0.27 s corresponding to a mass range of m/z 460 (\approx 920 mass channels, see

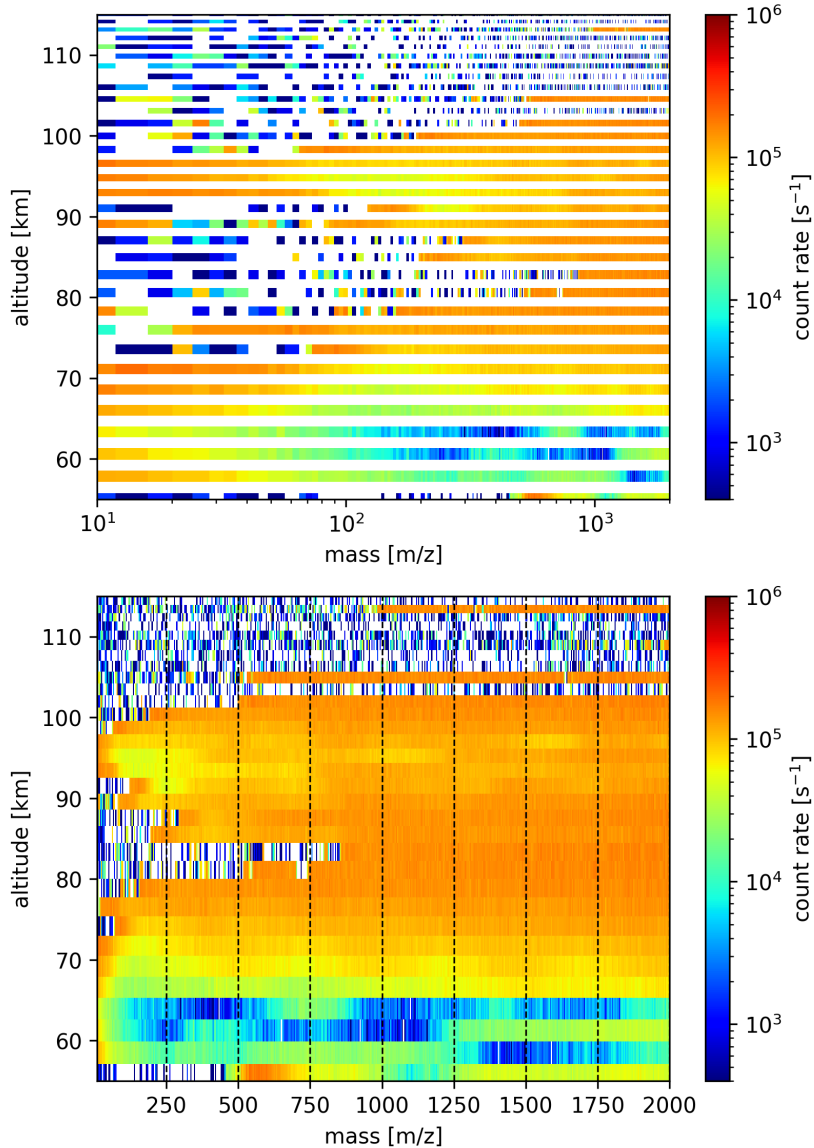


Figure 8. Negative ion spectra, during ascent of PMWE1F (ROMARA-1): Top panel with logarithmic mass scale, lower panel with linear mass scale and the positive measurement slots are filled with negative ion data for better visibility. Both plots have the full mass range.

210 Table 2) in the plots. The signal then disappears and appears with the last occurrence at 114 km. Lighter ions ($m/z < 150$) are visible at around 70 and 95 km but due to our limited mass resolution can not be resolved or are masked as the negative channels are in general more noisy because of a higher dark count rate compared to the positive spectra. A similar analysis as with the positive mass spectra could therefore not be done. For the available spectra no distinctive steps are produced, rather a slope due to the limited mass resolution, which indicates that more different ion types are involved as in the positive case.

215 Another feature is the absence of counts in the beginning of a spectrum between 75 and 90 km to varying masses, forming kind
of a zero signal in the plot of Fig.8, that is peaking at m/z 850 and 85 km. This behavior could be caused by a paralyzed detector
(Wüest et al., 2007), overwhelmed with particles of masses below the reappearance of counts, e.g. below m/z 850 at 85 km.
Thus we do not have continuous data for negative ions below m/z 150. Furthermore, the large negative ions exceeding our mass
220 the same altitude where the detector is paralyzed the most. The low saturating count rate could be caused by an increased dead
time due to large ions as reported by Vanhaecke et al. (1998) and Gemer et al. (2020).

The exact behavior of an individual ion detector to high numbers of different incident particles can be a very complex as
other parameters such as the pulse height distribution of the detector, aging or the threshold and dead time of the amplifier or
electronics can play a role.

225 **3.5 Negative ions ROMARA-2**

The negative ion measurements of ROMARA-2 show a large variety of ion masses and most importantly confirm the existence
of ions heavier than m/z 2000 as proposed before (Fig.9). Saturating effects as with ROMARA-1 are not existent, rather the
opposite which results in very low count rates of the lower sensitivity Mode B. The measurements can be broadly divided
in below and above 85 km. Below 85 km the mass spectra include in general large ions and show little to no ions below
230 m/z 100 which is unexpected when compared to ROMARA-1. The majority of detected ions is between m/z 200 and 1000,
at about 80 km up to m/z 5000 albeit with rather low count rates. Above 85 km the large ions disappear and lighter ions are
detected even in the lowest mass channels. Further, the unbiased mode with the intake cone at payload potential, does not show
counts anymore, either because of the lower masses and their lower energy or because of an increased payload potential, more
effectively shielding the negative ions. Above 100 km the count rates further decline due to the aerodynamic shielding effect.

235 **3.6 Background counts**

In the presented mass spectra, background counts are visible as incoherent counts, most obviously in the high mass channels
where the count rates are low or close to zero. The 1-count limit in the given binning of 8ch. or 32ch. is around 400 and 100, as
indicated by the lowest number of the color scale in Fig.6, 8, 7 and 9. Background counts are usually composed of dark noise
in the multiplier, penetrating radiation and UV-photons. In our data, we see the noise is increasing with altitude (e.g. upper
240 panel of Fig.7 and Appendix C, Fig.16). Dark noise should be constant and is usually in the range of some counts per minute
due to radioactive decay in the glass that it is made of and is therefore irrelevant for our measurements. As the detector is deeply
buried in the structure of the instrument and the payload, summing to a shielding of several millimeters of steel, copper and
aluminum, only cosmic rays could penetrate to the multiplier. This form of background noise is also in the range of only a few
counts per minute and we thus assume that scattered UV photons are the most likely cause of the background counts.

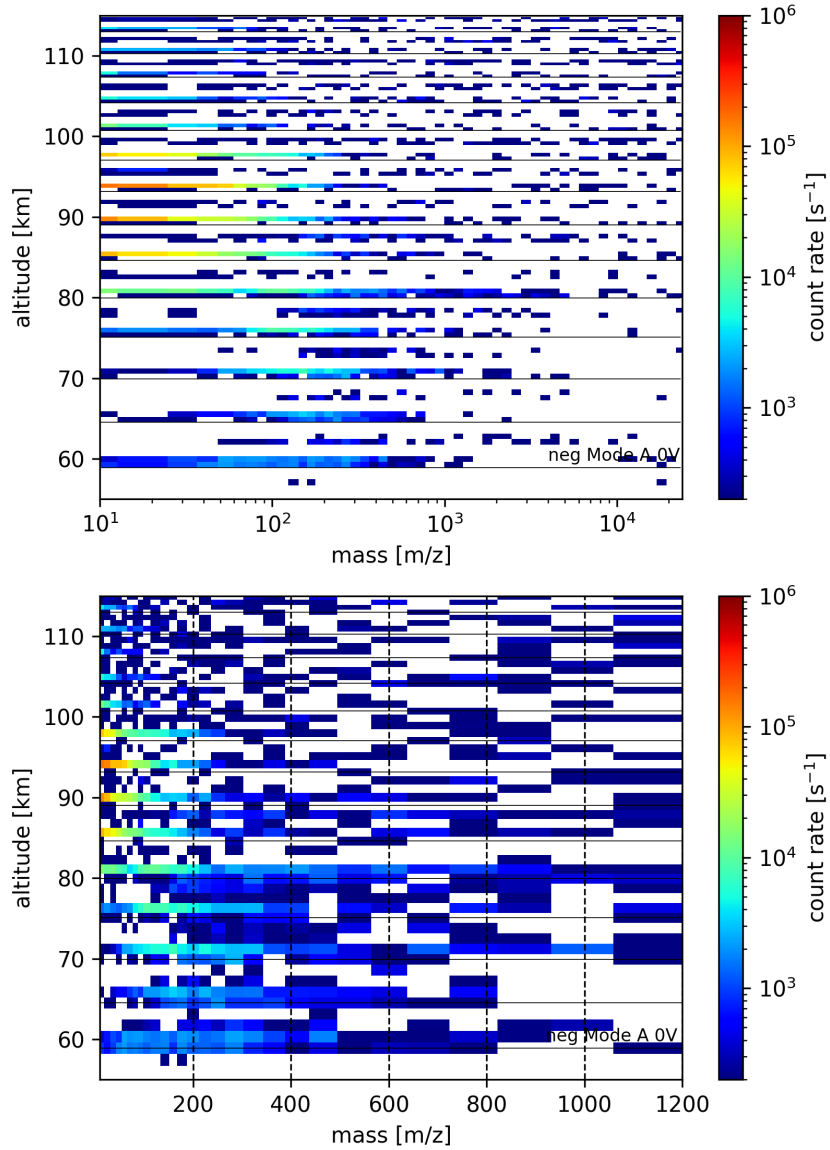


Figure 9. Negative ion spectra, during ascent of PMWE2F (ROMARA-2): Top panel with logarithmic mass scale and full mass range and 32ch. binning. The horizontal lines mark the nA0 measurement to indicate the measurement sequence (nA0, nA5, nB0, nB5). Positive ion measurements are omitted. The lower panel has a linear mass scale and the positive measurement slots are filled with negative ion data for better visibility.

The goal of the two flights was to detect and possibly identify the chemical nature of meteor smoke particles. The data of the ROMARA-1 flight did not show a significant signal for positive MSPs but suggested a large population of large negative particles of $> m/z$ 2000, albeit maybe being too sensitive and thus resulting in difficulties to interpret the negative spectra. ROMARA-2 showed, with high confidence, MSPs of both charge states. In order to identify possible meteor smoke compounds in our measurements we summarized the compounds proposed by Plane et al. (2014) and Hervig et al. (2017) in Table 5 and show their atomic mass up to multiples of 3 (trimer). One can see in Table 5, that e.g. MgO has such a small mass (40 u) that its multiples would fit almost any step in the higher mass ranges with the given mass resolution of ROMARA and thus makes unambiguous identification unfeasible.

Table 5. Compounds as possible building blocks of MSPs by Plane et al. (2014) and Hervig et al. (2017)

compound	mass [u] monomer	mass [u] dimer	mass [u] trimer	etc.
MgO[H]	40(41)	80(82)	120(123)	...
Mg(OH) ₂	58	116	174	...
FeO[H]	72(73)	144(146)	216(219)	...
Fe(OH) ₂	90	180	270	...
MgSiO ₃	100	200	300	...
FeSiO ₃	132	264	396	...
Mg ₂ SiO ₄	140	280	420	...
Fe ₂ O ₃	160	320	480	...
FeMgSiO ₄	172	344	516	...
Fe ₂ SiO ₄	204	408	612	...
Fe ₃ O ₄	232	464	696	...

For the discussion on the possible chemical composition of MSPs we focus on the most interesting altitudes from the individual ion spectra overview plots by averaging the mass spectra over selected altitudes. In the case of positive ions of both flights these are altitudes above the proton hydrates regime around 85 km which can be seen in the respective data. The negative ion data of the ROMARA-2 flight are examined in the same altitude range but we also analyze lower altitudes including some interesting mass spectra.

4.1 Discussion positive ions ROMARA-1

The most interesting altitudes for MSPs in the ROMARA-1 data are the altitudes between the iron peak at 89.6, 91.5 and 93.4 km (Fig.6). The mean spectrum from these 3 altitudes is plotted in Fig.10 up to m/z 120. One can see the aforementioned NO^+/O_2^+ and Fe^+ peak (Reid, 1977; Shuman et al., 2015; Plane et al., 2015; Kopp et al., 1984). In between these

peaks, potential signatures of $\text{NO}^+\text{H}_2\text{O}$ are visible. Very few counts between m/z 70 and 100, could indicate NO^+CO_2 [74u], $\text{FeO}[\text{H}]$ [72u/73u] or $\text{Fe}(\text{OH})_2$ [90u] as modeled by Reid (1977) but no traces of heavier ions. The picture retrieved by the instrument for positive ions thus represents a rather expected ion population, with no large positive ions or MSPs above our sensitivity level.

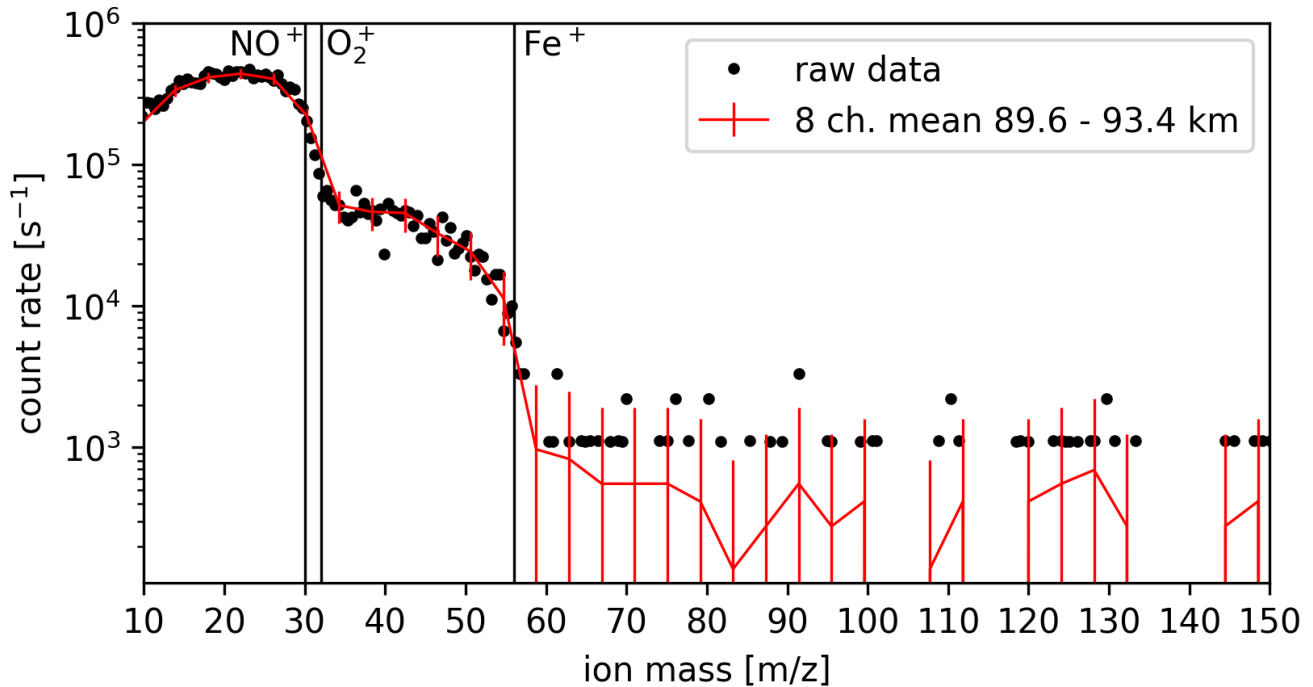


Figure 10. Mass spectrum for positive ions up to m/z 120 as mean between 89.6 to 93.4 km altitude during ascent of flight PMWE1F (ROMARA-1).

4.2 Discussion positive ions ROMARA-2

Despite that ROMARA-2 was able to measure down to m/z 20-30 the data below about m/z 150 suffers from a larger mass number uncertainty due to the large mass range setting. The results for masses below about m/z 150 are therefore slightly shifted towards higher values as we did not aim for those masses but still wanted to see if ions are present, e.g. NO^+ and Fe^+ .

In Fig.7 a very interesting feature between 96.3 and 100.4 km can be seen that are likely MSPs. We plot the mean of all 6 positive mass spectra between 96.3 - 100.4 km altitude up to m/z 1000 in Fig.11. Besides the raw 8 channel data, we plot a binned set of 32 mass channels which roughly correlates to the mass resolution and provides smoother data and is the basis of a differential spectrum. The differential spectrum is derived by subtracting subsequent channels $\Delta c = ch_n - ch_{n+1}$ and in case of a positive slope the data is omitted. The bins with the highest count rates above m/z 150 are centered around m/z 188, 237 and 302.

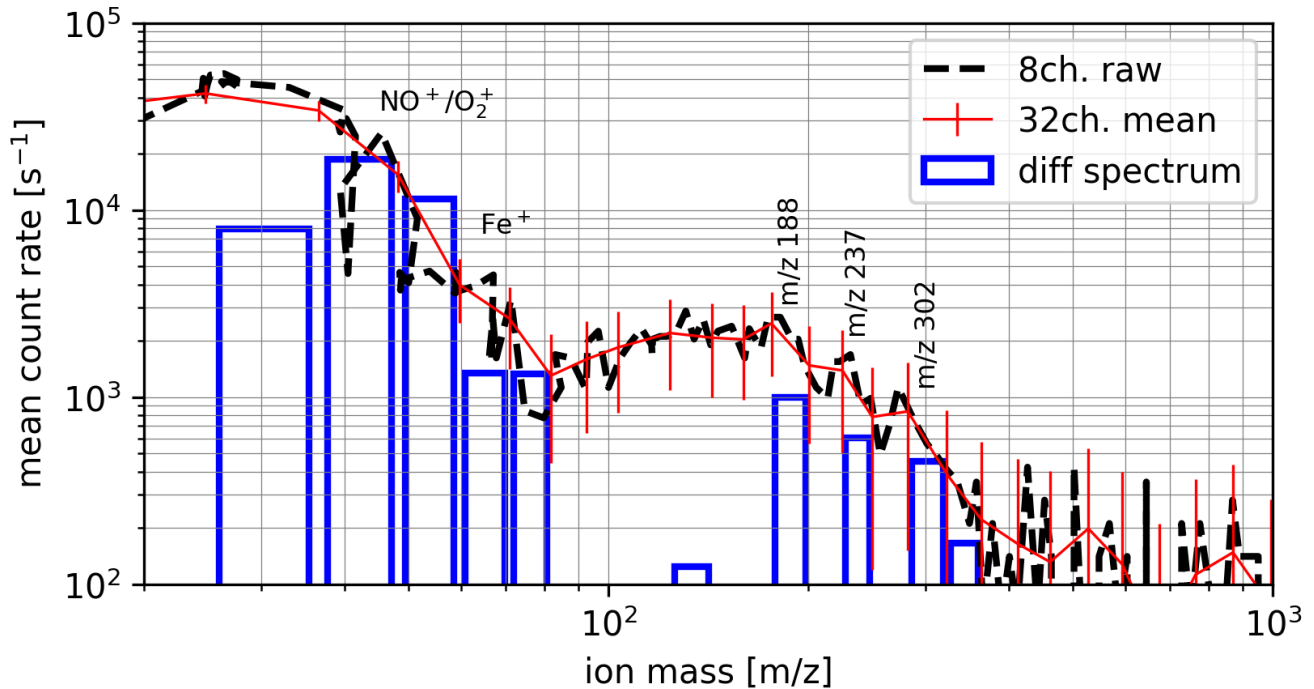


Figure 11. Mean mass spectra of all positive ion measurements of PMWE2F (ROMARA-2) between 96.3 - 100.4 km up to m/z 1000. Note the slightly drifted peaks for NO^+ and Fe^+ . The differential bins above m/z 150 are marked with their center mass per charge.

From Table 5 we looked at possible matches to the most probable bins we measured and show these matches in Table 6. For the mass bin m/z 188 we found $(\text{Fe}(\text{OH})_2)_2[180\text{u}]$ or $(\text{MgSiO}_3)_2[200\text{u}]$, where the iron hydroxide seems to fit best as the count rate drops clearly before m/z 200. In general one might argue that compounds of lower indexes < 3 , are probably more likely to exist and thus e.g. in the case of m/z 237, Fe_3O_4 might be a stronger candidate than $(\text{MgO}[\text{H}])_6$. But whether $(\text{Fe}_2\text{O}_3)_2$ is more likely as $(\text{MgSiO}_3)_3$, we cannot say, except that in the same spectra plenty of iron ions are available and thus the corresponding compounds might prevail.

Table 6. Mass bins of major steps in positive mass spectra between 96.3 and 100.4 km

mass bin	MSP compound
188	$(\text{Fe}(\text{OH})_2)_2$, $(\text{MgSiO}_3)_2$
237	Fe_3O_4 , $(\text{Mg}(\text{OH})_2)_4$, $(\text{MgO}[\text{H}])_6$
302	$(\text{MgO}[\text{H}])_7$, $(\text{Mg}(\text{OH})_2)_5$, $(\text{FeO}[\text{H}])_4$ $(\text{MgSiO}_3)_3$, $(\text{Fe}_2\text{O}_3)_2$

4.3 Discussion negative ions ROMARA-2

As mentioned before the negative ion measurements show basically two different regions, above and below 85 km. To begin
285 with, we compare the negative ion measurements with the positive ion layer around 97 km, by taking the average of counts
between 89.7 and 97.7 km in the same way as for the positive ion case. At these altitudes only the biased Mode A (n5A)
produced significant count rates of similar masses as the positive ions. The mean negative ion spectrum from 89.7, 93.9
and 97.7 km altitude is plotted in Fig.12, showing much more peaks compared to the positive ion spectra, which makes
290 and individual steps overlap. For a spectrum of low mass resolution with many different steps, the spectrum turns into a slope
and individual steps overlap.

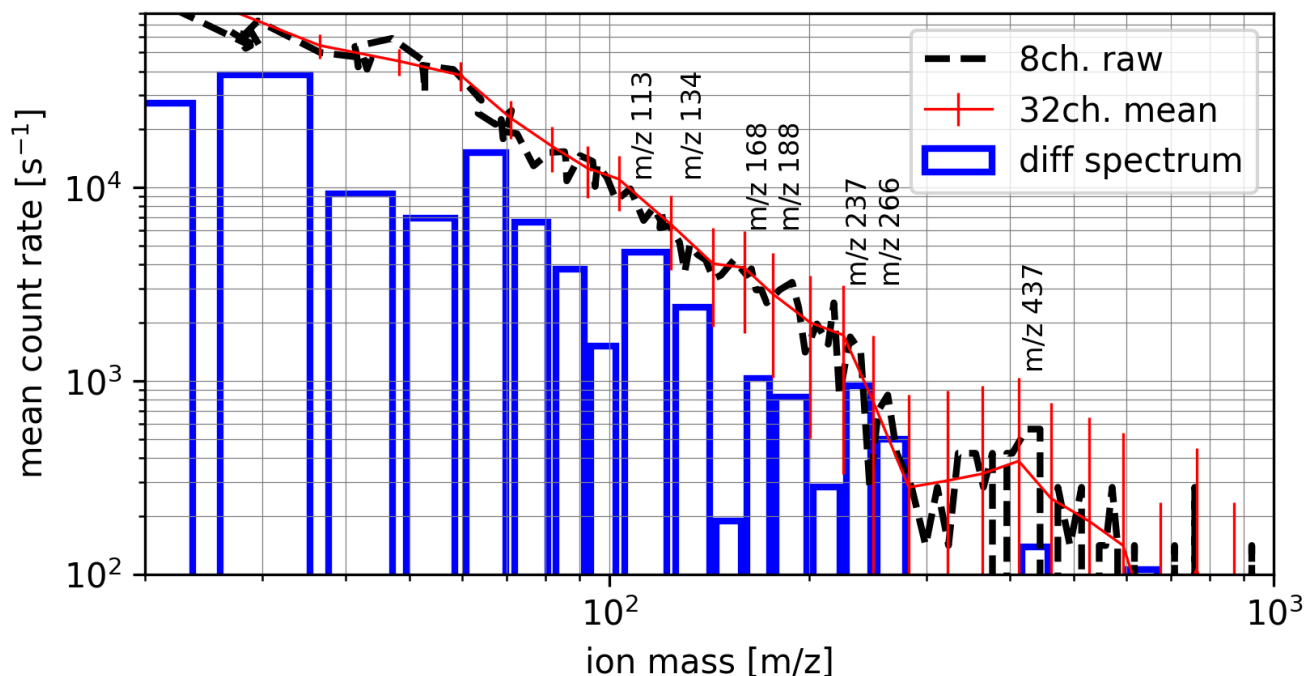


Figure 12. Mean mass spectra of negative ion measurements of mode n5A at 89.7, 93.9 and 97.7 km up to m/z 1000 from PMWE2F (ROMARA-2). The bins of interest are marked with their center mass per charge.

Nevertheless the possible compounds are given in Table 7. Between the possible compounds of each bin we cannot distinguish and others might rule out certain compounds. An interesting observation are the compounds Mg_2SiO_4 and $Fe(OH)_2$, occurring more often as possible matches, with Mg_2SiO_4 showing the smallest index number (trimer). The opposite is the case for $FeO[H]$, which is only once a possible match, albeit having a high probability according to Hervig et al. (2017). Thus we
295 find that Mg_2SiO_4 (Forsterite) is the most likely negative MSP compound for our measurements.

Table 7. mass bins of major steps in negative mass spectra between 89.7 and 97.7 km

mass bin	MSP compound
113	(Mg(OH) ₂) ₂ , (MgO[H]) ₃
134	FeSiO ₃ , Mg ₂ SiO ₄
166	Fe ₂ O ₃ , (MgO[H]) ₄ , FeMgSiO ₄ , (Mg(OH) ₂) ₃
188	(Fe(OH) ₂) ₂ , (MgSiO ₃) ₂
237	Fe ₃ O ₄ , (Mg(OH) ₂) ₄ , (MgO[H]) ₆
266	(FeSiO ₃) ₂ , (Fe(OH) ₂) ₃ , (MgSiO ₄) ₂
437	(MgSiO ₄) ₃ , (Fe(OH) ₂) ₅ , (FeO[H]) ₆ , (MgO[H]) ₁₁

In Fig.13 we present 3 interesting spectra: panel a) shows a pattern of multiplying masses at 80.8 km, panel b) shows the heaviest detected mass at 80.2 km and panel c) corresponds to the altitude of the radar echo at 65.6 km, as this echo was a launch condition. The pattern in panel a) shows distinctive steps at roughly m/z 225, 450, 900 and 1800, that could indicate a compound that is doubling its mass. This pattern is not correlated to the payload spin, as the time between these mass channels is roughly 100 ms and the payload spins at 3.6 Hz (277 ms) Further we do not expect proton hydrates above $m/z > 400$, as proton hydrates seem to have a maximum of about 20 ligands (361 u) (Björn and Arnold, 1981). If we ignore the smaller hydroxides and oxides we arrive at 2 possible compounds as plotted in panel a) with vertical lines: Fe₃O₄ and Fe₂SiO₄ as monomer, dimer and tetramer, possibly even as octomer Thus we might have detected Magnetite (iron oxide) or Fayalite cluster MSPs. This aligns well with the measurements and results of Hervig et al. (2017): "The most likely MSP compositions are magnetite (Fe₃O₄), wüstite (FeO), and iron-rich olivine (Fayalite, Fe₂SiO₄)".

Panel b) shows the heaviest recorded signals reaching up to m/z 5500. As the count rate is low, we refrain from assigning possible compounds but it seems that the signal between about m/z 1000 and 5500 besides being noisy does not show a typical tail, thus indicating a single compound at about m/z 5000 is producing the counts. This partly confirms the measurements of ROMARA-1 and the possibility of ions with masses above m/z 2000 although it does not explain the general observation during the flight of ROMARA-1 with a layer of large negative ions, spanning from about 65 to 100 km.

In panel c) we show the spectrum at 65.5 km, where the PMWE echo was detected. In the same way as before we found significant steps at the mass bins: m/z 188, 237 and 343 albeit the compounds at this lower altitudes could be different from above 85 km Thus for the first bin: (Fe(OH)₂)₂ or (MgSiO₃)₂, for the second bin: Fe₃O₄, (Mg(OH)₂)₄ or (MgO[H])₆ and for the third: (MgO[H])₈, (Mg(OH)₂)₆, (FeO[H])₅ and (Fe(OH)₂)₄ or (FeMgSiO₄)₂. The maximum mass in this case is m/z 500 to 600. Thus the composition at this altitude does not differ significantly from other spectra, just below or above. An interesting RF-only spectrum for negative ions is given in Schulte and Arnold (1992) using a similar instrument at 77.6 km (Kiruna, 3rd August 1982, night time) with mass steps around 160 u, 250 u and 330 u indicating similar ions as observed with ROMARA-2.

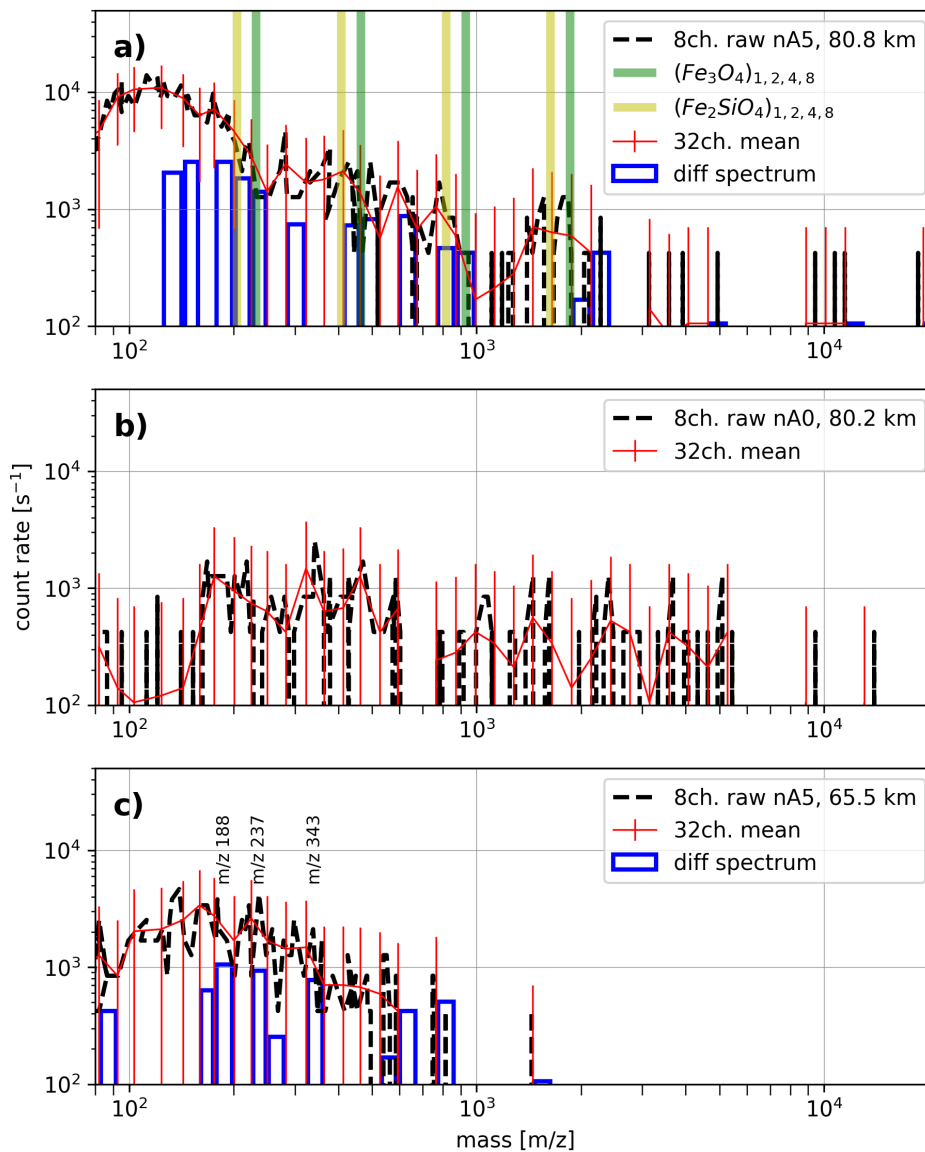


Figure 13. Spectra of negative ions from ROMARA-2 for the region of present PMWE (c) and of the heaviest mass signals (a,b) (PMWE2F).

5 Summary

320 The picture we received from our two flights is ambiguous. Concerning positive ions during the ROMARA-1 flight we measured a somewhat expected population of proton hydrates and NO^+/O_2^+ , although some signs of other metal ions are missing, e.g. Mg^+ (Plane and Whalley, 2012) or Si^+ (Plane et al., 2016) but no ions above about m/z 100. The ROMARA-2 data essentially shows the same picture but has an additional positive ion population between m/z 180 and 350 included at unexpected

high altitudes between 96.3 - 100.4 km. This unexpected layer shows a number of possible compounds, indicating a diverse
325 chemical composition, most likely revolving around iron as the most abundant metal ion.

Concerning the negative ion measurements we did not receive a clear picture from the ROMARA-1 data as our measurement
was saturated with ions of $m/z > 2000$. ROMARA-2 data could confirm that particles of such mass per charge ratio exist but
the mass range was not well suited for masses below $m/z 150$. The limited mass resolution of the ROMARA-2 measurements
due to the selected large mass range further restricted our analysis. However, our observations seem to be in line with the
330 measurements of Hervig et al. (2017) further backing up his proposed "magnetite, wüstite, and iron-rich olivine". Rapp et al.
(2012) proposed metal hydroxides eg. MgOH and FeOH in favour of silicates which we could neither confirm nor reject
for the reasons mentioned above. The overall picture from our measurements of possible compounds in MSP show a zoo of
possibilities and it seems clear that there is no single MSP compound apart from a likely iron dominated chemical composition
as proposed by others in the MLT region. Unambiguously identification would require a next generation rocket-borne mass
335 spectrometer with a mass resolution capable of distinguishing e.g. $(\text{FeO})_4[288\text{u}]$ from $(\text{FeOH})_4[292\text{u}]$.

6 Appendix A: Intake cone current

The intake cone current is measured with high resolution as an absolute value during the flight and is the net sum of all
charge carriers interacting on it. As the cone of ROMARA-1 was on payload potential (0 V) only one curve is obtained, while
ROMARA-2 had 3 different potentials (0, +5 (neg) and -5 V (pos)), as shown in Fig.14.

340 7 Appendix B: Payload charging

An object in a plasma charges to a certain potential, such as a payload in the MLT region. Mass spectra allow to estimate the
payload potential if enough ions of the right mass are present, i.e. if an ion mass is present in the 5 V mode, but absent in the
0 V mode, then the payload potential (V_p) must be larger than:

$$V_p > \frac{m}{2e} v^2, \quad (3)$$

345 with m as ion mass and v as payload speed. The same must be true if in both modes an ion mass is present and thus the
payload potential must be smaller than $\frac{m}{2e} v^2$. At 60 km in Fig.15 the difference in count rate between 0 and 5 V at the intake is
minimal, thus a payload potential for detected ions around $m/z 100$ does not have an influence and gives a maximum payload
potential of around -0.65 V as 100 u (lighter ions are a bit uncertain) ions would overcome the energy barrier given the payload
potential. At 76 km ions of $m/z 220$ or 320 enter the instrument at comparable count rates for 0 V and 5 V, indicating a payload
350 potential of around -1.1 to -1.6 V. At 85 km ions of about $m/z 450$ are present in the 5 V mode but not in the 0 V mode, thus
indicating a payload potential of at least -1.8 V. Thus the payload is charging up increasingly negatively to about -2 Volts as
usually anticipated and previously measured by e.g. Bekkeng et al. (2013).

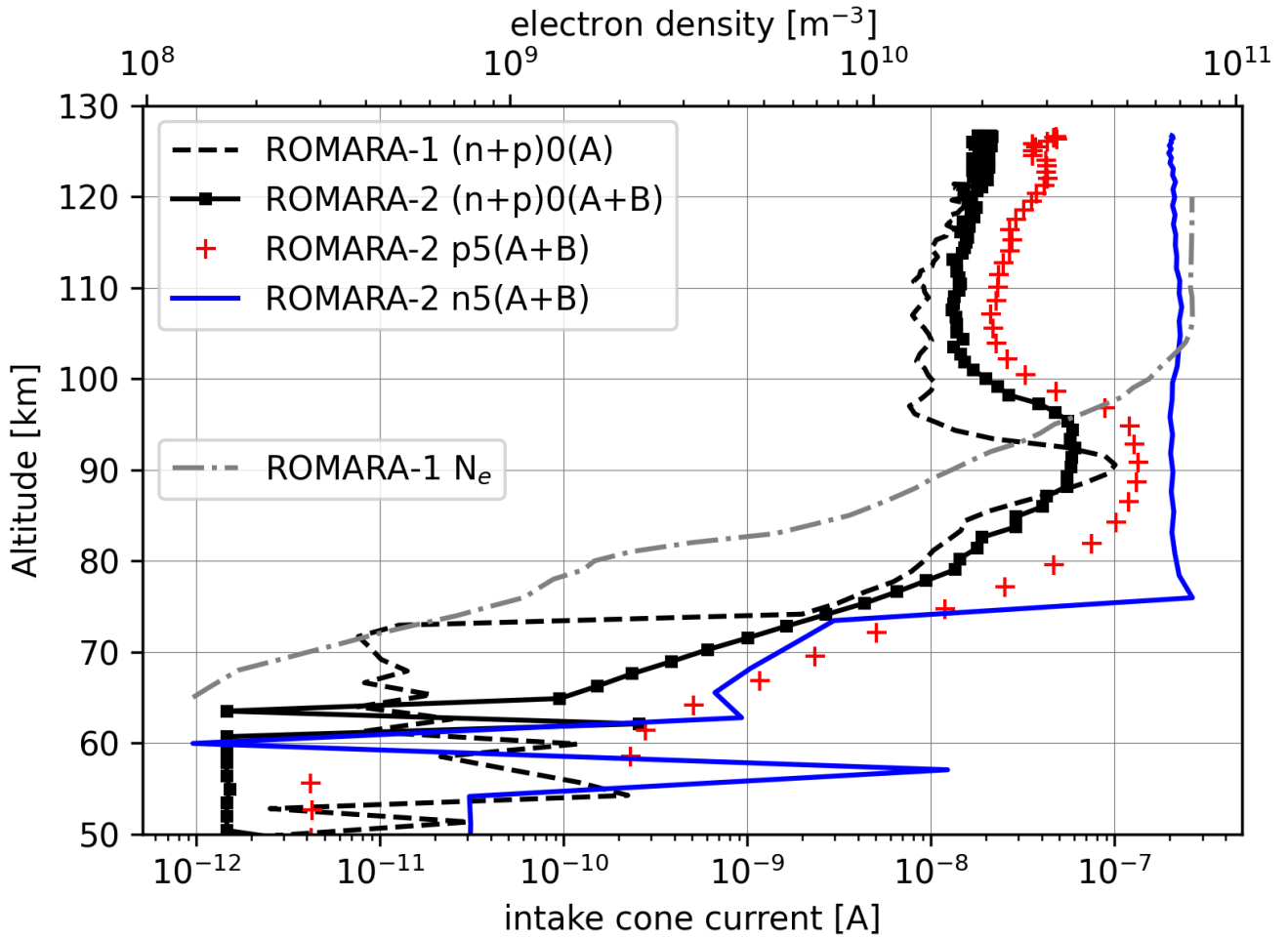


Figure 14. Intake cone current mean values over whole spectrum for ROMARA-1 and ROMARA-2. The electron density N_e from ROMARA-1 is added with data from Staszak et al. (2021).

8 Appendix C: Background counts ROMARA-2

To illustrate the background counts we show in Fig.16 the mean count rate of masses above m/z 6000 for positive and negative channels, not separated by Mode A and B but with different intake cone potentials. The symmetry between ascent and descent is a strong indicator that these counts are not caused by particles as the instrument is in the wake during descent as indicated by the angle of attack. The similarity between the different intake cone potentials also indicate no particle involvement. Furthermore correlates the count rate with increasing altitude and thus UV light intensity.

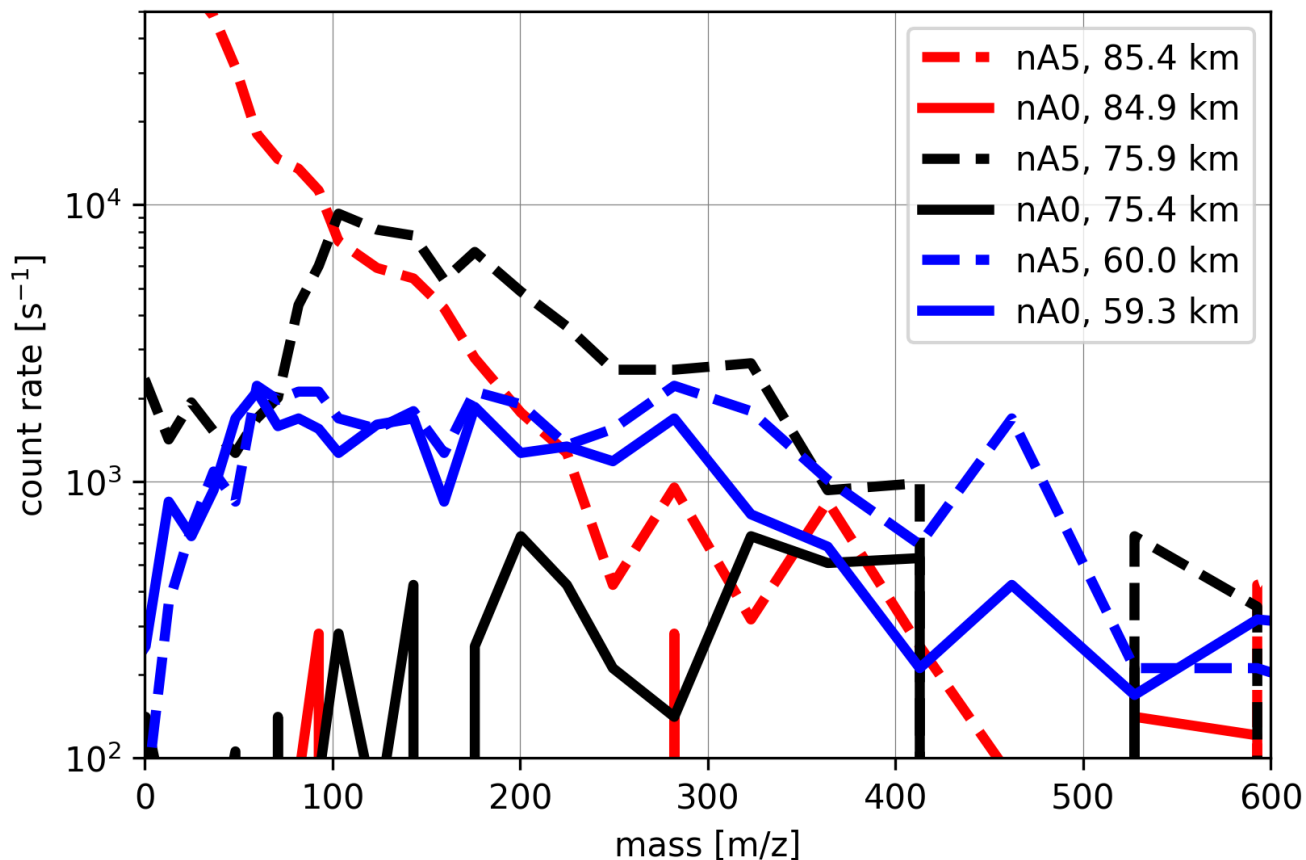


Figure 15. Spectra of negative ions for 0 and 5 V potentials at the intake cone, showing 3 different cases, to estimate the payload potential.

Data availability. ROMARA-1 data is available at: <https://zenodo.org/doi/10.5281/zenodo.11470114> (Stude et al., 2020)

360 ROMARA-2 data is available at: <https://zenodo.org/doi/10.5281/zenodo.11469720> (Stude et al., 2024)

The data files should be self explanatory.

Author contributions. JS prepared the instrument (CoPI), analysed the data and drafted the manuscript

HA prepared the instrument

HS supervision

365 MR supervision and instrument PI

FA supervision

BS PMWE project PI

CB ion compositions and payload charging

All authors actively contributed to the discussions and to writing the final version of the paper.

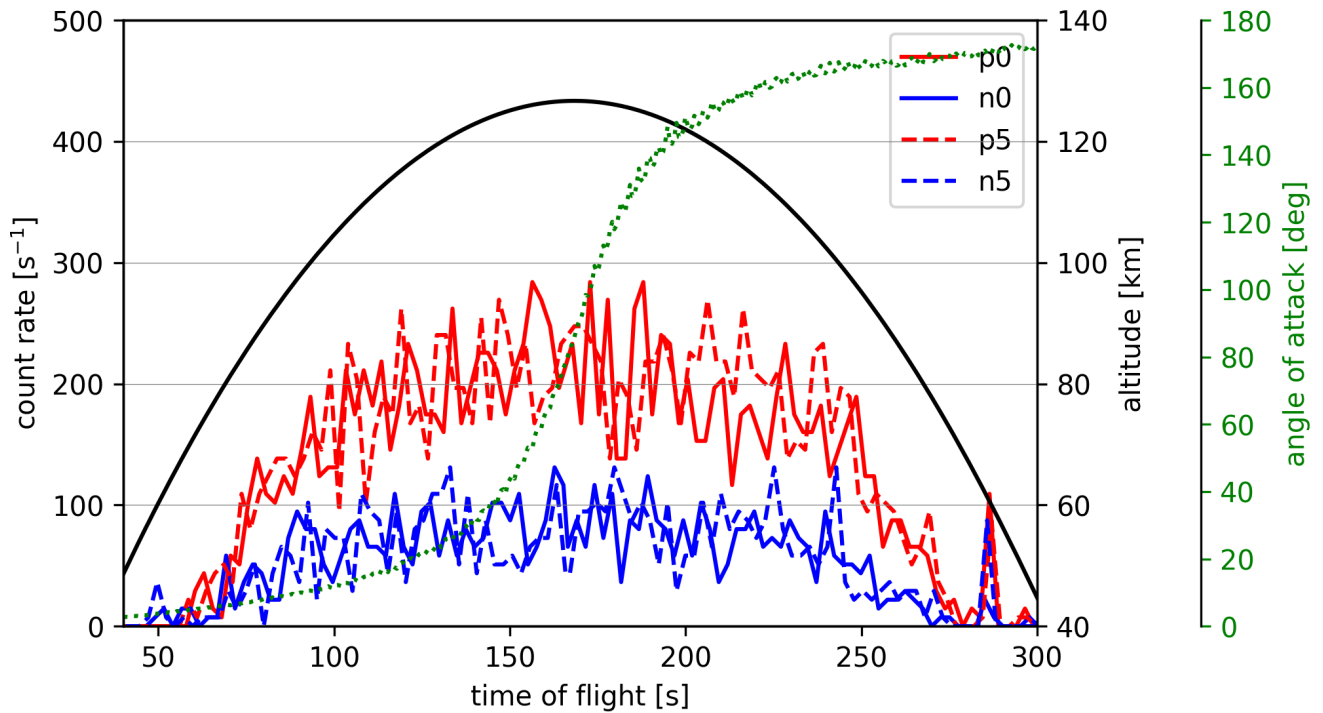


Figure 16. Mean count rate from ROMARA-2 for masses above m/z 6000 for positive and negative channels.

370 *Competing interests.* The authors declare that they have no conflict of interest

Acknowledgements. Project PMWE was funded by the German Federal Ministry for Economic Affairs and Energy and funded by the German Space Agency (DLR) under grant 50OE1402. We further like to thank the mobile rocket base (MORABA) and Andøya Space Center (ASC) for their intense and kind support as well as Robert Lindemann and Matthias Lang for their excellent technical work.

References

- 375 Agilent: Certificate of Analysis ESI-L Low Concentration Tuning Mix 100ml Agilent Part Number: G1969-85000 Sample Lot Number: LB86189, <https://www.agilent.com/cs/library/certificateofanalysis/G1969-85000cofa872022-U-LB86189.pdf>, accessed: 2023-02-15.
- Antonsen, T., Havnes, O., and Spicher, A.: Multi-scale measurements of mesospheric aerosols and electrons during the MAXIDUSTY campaign, *Atmospheric Measurement Techniques*, 12, 2139–2153, <https://doi.org/10.5194/amt-12-2139-2019>, 2019.
- Asmus, H., Staszak, T., Strelnikov, B., Lübken, F.-J., Friedrich, M., and Rapp, M.: Estimate of size distribution of charged MSPs measured
380 in situ in winter during the WADIS-2 sounding rocket campaign, *Annales Geophysicae*, 35, 979–998, <https://doi.org/10.5194/angeo-35-979-2017>, 2017.
- Baumann, C., Rapp, M., Anttila, M., Kero, A., and Verronen, P. T.: Effects of meteoric smoke particles on the D region ion chemistry, *Journal of Geophysical Research: Space Physics*, 120, 10,823–10,839, <https://doi.org/10.1002/2015JA021927>, 2015.
- Bekkeng, T. A., Barjatya, A., Hoppe, U.-P., Pedersen, A., Moen, J. I., Friedrich, M., and Rapp, M.: Payload charging events in the mesosphere
385 and their impact on Langmuir type electric probes, *Annales Geophysicae*, 31, 187–196, <https://doi.org/10.5194/angeo-31-187-2013>, 2013.
- Björn, L. G. and Arnold, F.: Mass spectrometric detection of precondensation nuclei at the Arctic summer mesopause, *Geophysical Research Letters*, 8, 1167–1170, <https://doi.org/https://doi.org/10.1029/GL008i011p01167>, 1981.
- Chesworth, E. T. and Hale, L. C.: Ice particulates in the mesosphere, *Geophysical Research Letters*, 1, 347–350, <https://doi.org/10.1029/GL001i008p00347>, 1974.
- 390 Gelinás, L. J., Lynch, K. A., Kelley, M. C., Collins, S., Baker, S., Zhou, Q., and Friedman, J. S.: First observation of meteoritic charged dust in the tropical mesosphere, *Geophysical Research Letters*, 25, 4047–4050, <https://doi.org/10.1029/1998GL900089>, 1998.
- Gemer, A., Sternovsky, Z., James, D., and Horanyi, M.: The effect of high-velocity dust particle impacts on microchannel plate (MCP) detectors, *Planetary and Space Science*, 183, 104 628, <https://doi.org/https://doi.org/10.1016/j.pss.2018.12.011>, special issue on Cosmic Dust X, 2020.
- 395 Havnes, O., Antonsen, T., Hartquist, T., Fredriksen, Å., and Plane, J.: The Tromsø programme of in situ and sample return studies of mesospheric nanoparticles, *Journal of Atmospheric and Solar-Terrestrial Physics*, 127, 129 – 136, <https://doi.org/10.1016/j.jastp.2014.09.010>, 2015.
- Hervig, M. E., Brooke, J. S. A., Feng, W., Bardeen, C. G., and Plane, J. M. C.: Constraints on Meteoric Smoke Composition and Meteoric Influx Using SOFIE Observations With Models, *Journal of Geophysical Research: Atmospheres*, 122, 13,495–13,505,
400 <https://doi.org/10.1002/2017JD027657>, 2017.
- Hunten, D. M., Turco, R. P., and Toon, O. B.: Smoke and Dust Particles of Meteoric Origin in the Mesosphere and Stratosphere, *Journal of the Atmospheric Sciences*, 37, 1342–1357, [https://doi.org/10.1175/1520-0469\(1980\)037<1342:SADPOM>2.0.CO;2](https://doi.org/10.1175/1520-0469(1980)037<1342:SADPOM>2.0.CO;2), 1980.
- Johannessen, A., Krankowsky, D., Arnold, F., Riedler, W., Friedrich, M., Folkestad, K., Skovli, G., Thrane, E. V., and Tröim, J.: Physical Sciences: Detection of Water Cluster Ions at the High Latitude Summer Mesopause, *Nature*, 235, 215–217, <https://doi.org/10.1038/235215a0>,
405 1972.
- Kopp, E., Ramseyer, H., and Björn, L.: Positive ion composition and electron density in a combined auroral and NLC event, *Advances in Space Research*, 4, 157 – 161, [https://doi.org/10.1016/0273-1177\(84\)90279-5](https://doi.org/10.1016/0273-1177(84)90279-5), 1984.
- Latteck, R. and Strelnikova, I.: Extended observations of polar mesosphere winter echoes over Andøya (69°N) using MAARSY, *Journal of Geophysical Research: Atmospheres*, 120, 8216–8226, <https://doi.org/10.1002/2015JD023291>, 2015.

- 410 Latteck, R., Renkwitz, T., and Strelnikov, B.: D region observations by VHF and HF radars during a rocket campaign at Andøya dedicated to investigations of PMWE, *Advances in Radio Science*, 17, 225–237, <https://doi.org/10.5194/ars-17-225-2019>, 2019.
- Lynch, K. A., Gelinas, L. J., Kelley, M. C., Collins, R. L., Widholm, M., Rau, D., MacDonald, E., Liu, Y., Ulwick, J., and Mace, P.: Multiple sounding rocket observations of charged dust in the polar winter mesosphere, *Journal of Geophysical Research: Space Physics*, 110, <https://doi.org/10.1029/2004JA010502>, 2005.
- 415 Megner, L., Siskind, D. E., Rapp, M., and Gumbel, J.: Global and temporal distribution of meteoric smoke: A two-dimensional simulation study, *Journal of Geophysical Research: Atmospheres*, 113, <https://doi.org/10.1029/2007JD009054>, 2008.
- Obenberger, K. S., Holmes, J. M., Ard, S. G., Dowell, J., Shuman, N. S., Taylor, G. B., Varghese, S. S., and Viggiano, A. A.: Association Between Meteor Radio Afterglows and Optical Persistent Trains, *Journal of Geophysical Research: Space Physics*, 125, e2020JA028053, <https://doi.org/10.1029/2020JA028053>, 2020.
- 420 Paul, W. and Steinwedel, H.: Notizen: Ein neues Massenspektrometer ohne Magnetfeld, *Zeitschrift für Naturforschung A*, 8, 448–450, <https://doi.org/doi:10.1515/zna-1953-0710>, 1953.
- Plane, J. M., Saunders, R. W., Hedin, J., Stegman, J., Khaplanov, M., Gumbel, J., Lynch, K. A., Bracikowski, P. J., Gelinas, L. J., Friedrich, M., Blindheim, S., Gausa, M., and Williams, B. P.: A combined rocket-borne and ground-based study of the sodium layer and charged dust in the upper mesosphere, *Journal of Atmospheric and Solar-Terrestrial Physics*, 118, 151–160, <https://doi.org/10.1016/j.jastp.2013.11.008>, 425 2014.
- Plane, J. M. C. and Whalley, C. L.: A New Model for Magnesium Chemistry in the Upper Atmosphere, *The Journal of Physical Chemistry A*, 116, 6240–6252, <https://doi.org/10.1021/jp211526h>, PMID: 22229654, 2012.
- Plane, J. M. C., Feng, W., and Dawkins, E. C. M.: The Mesosphere and Metals: Chemistry and Changes, *Chemical Reviews*, 115, 4497–4541, <https://doi.org/10.1021/cr500501m>, PMID: 25751779, 2015.
- 430 Plane, J. M. C., Gómez-Martín, J. C., Feng, W., and Janches, D.: Silicon chemistry in the mesosphere and lower thermosphere, *Journal of Geophysical Research: Atmospheres*, 121, 3718–3728, <https://doi.org/10.1002/2015JD024691>, 2016.
- Plane, J. M. C., Gumbel, J., Kalogerakis, K. S., Marsh, D. R., and von Savigny, C.: Opinion: Recent developments and future directions in studying the mesosphere and lower thermosphere, *Atmospheric Chemistry and Physics*, 23, 13 255–13 282, <https://doi.org/10.5194/acp-23-13255-2023>, 2023.
- 435 Rapp, M., Hedin, J., Strelnikova, I., Friedrich, M., Gumbel, J., and Lübken, F.-J.: Observations of positively charged nanoparticles in the nighttime polar mesosphere, *Geophysical Research Letters*, 32, <https://doi.org/10.1029/2005GL024676>, 2005.
- Rapp, M., Plane, J. M. C., Strelnikov, B., Stober, G., Ernst, S., Hedin, J., Friedrich, M., and Hoppe, U.-P.: In situ observations of meteor smoke particles (MSP) during the Geminids 2010: constraints on MSP size, work function and composition, *Annales Geophysicae*, 30, 1661–1673, <https://doi.org/10.5194/angeo-30-1661-2012>, 2012.
- 440 Reid, G. C.: The production of water-cluster positive ions in the quiet daytime D region, *Planetary and Space Science*, 25, 275–290, [https://doi.org/https://doi.org/10.1016/0032-0633\(77\)90138-6](https://doi.org/https://doi.org/10.1016/0032-0633(77)90138-6), 1977.
- Robertson, S., Dickson, S., Horányi, M., Sternovsky, Z., Friedrich, M., Janches, D., Megner, L., and Williams, B.: Detection of meteoric smoke particles in the mesosphere by a rocket-borne mass spectrometer, *Journal of Atmospheric and Solar-Terrestrial Physics*, 118, 161 – 179, <https://doi.org/10.1016/j.jastp.2013.07.007>, 2014.
- 445 Rosinski, J. and Snow, R. H.: SECONDARY PARTICULATE MATTER FROM METEOR VAPORS, *Journal of Meteorology*, 18, 736–745, [https://doi.org/10.1175/1520-0469\(1961\)018<0736:SPMFMV>2.0.CO;2](https://doi.org/10.1175/1520-0469(1961)018<0736:SPMFMV>2.0.CO;2), 1961.

- Schulte, P. and Arnold, F.: Detection of upper atmospheric negatively charged microclusters by a rocket-borne mass spectrometer, *Geophysical Research Letters*, 19, 2297–2300, <https://doi.org/10.1029/92GL02631>, 1992.
- Shuman, N. S., Hunton, D. E., and Viggiano, A. A.: Ambient and Modified Atmospheric Ion Chemistry: From Top to Bottom, *Chemical Reviews*, 115, 4542–4570, <https://doi.org/10.1021/cr5003479>, PMID: 25659834, 2015.
- 450 Staszak, T., Strelnikov, B., Latteck, R., Renkwitz, T., Friedrich, M., Baumgarten, G., and Lübken, F.-J.: Turbulence generated small-scale structures as PMWE formation mechanism: Results from a rocket campaign, *Journal of Atmospheric and Solar-Terrestrial Physics*, 217, 105 559, <https://doi.org/https://doi.org/10.1016/j.jastp.2021.105559>, 2021.
- Strelnikov, B., Szewczyk, A., and Rapp, M.: In-situ measurements of small-scale structures in neutrals and plasma species during ECOMA-2010, in: *EGU General Assembly Conference Abstracts*, edited by Abbasi, A. and Giesen, N., vol. 14 of *EGU General Assembly Conference Abstracts*, p. 11861, <https://ui.adsabs.harvard.edu/abs/2012EGUGA..1411861S>, 2012.
- 455 Strelnikov, B., Staszak, T., Latteck, R., Renkwitz, T., Strelnikova, I., Lübken, F.-J., Baumgarten, G., Fiedler, J., Chau, J. L., Stude, J., Rapp, M., Friedrich, M., Gumbel, J., Hedin, J., Belova, E., Hörschgen-Eggers, M., Giono, G., Hörner, I., Löhle, S., Eberhart, M., and Fasoulas, S.: Sounding rocket project “PMWE” for investigation of polar mesosphere winter echoes, *Journal of Atmospheric and Solar-Terrestrial*
- 460 *Physics*, 218, 105 596, <https://doi.org/10.1016/j.jastp.2021.105596>, 2021.
- Stude, J., Aufmhoff, H., and Rapp, M.: PMWE1F-ROMARA, <https://doi.org/10.5281/zenodo.11470114>, 2020.
- Stude, J., Aufmhoff, H., Schlager, H., Rapp, M., Arnold, F., and Strelnikov, B.: A novel rocket-borne ion mass spectrometer with large mass range: instrument description and first-flight results, *Atmospheric Measurement Techniques*, 14, 983–993, <https://doi.org/10.5194/amt-14-983-2021>, 2021.
- 465 Stude, J., Aufmhoff, H., and Rapp, M.: PMWE2F-ROMARA, <https://doi.org/10.5281/zenodo.11469720>, 2024.
- Vanhaecke, F., de Wannemacker, G., Moens, L., Dams, R., Latkoczy, C., Prohaska, T., and Stingeder, G.: Dependence of detector dead time on analyte mass number in inductively coupled plasma mass spectrometry, *J. Anal. At. Spectrom.*, 13, 567–571, <https://doi.org/10.1039/A709001C>, 1998.
- Wüest, M., Evans, D., and von Steiger, R.: Calibration of Particle Instruments in Space Physics, p. 132, 2007.
- 470 Zbinden, P., Hidalgo, M., Eberhahdt, P., and Geiss, J.: Mass spectrometer measurements of the positive ion composition in the D- and E-regions of the ionosphere, *Planetary and Space Science*, 23, 1621–1642, [https://doi.org/https://doi.org/10.1016/0032-0633\(75\)90090-2](https://doi.org/https://doi.org/10.1016/0032-0633(75)90090-2), 1975.